Supporting Information

Hysteretic Gas and Vapor Sorption in Flexible Interpenetrated Lanthanide-based Metal-Organic Frameworks with Coordinated Molecular Gating via Reversible Single-Crystal to Single-Crystal Transformation for Enhanced Selectivity

Chao Wang[1,3,4], Liangjun Li[1], Jon G. Bell[2], Xiaoxia Lv[3,5], Sifu Tang[3], Xuebo Zhao[1,3*], K Mark Thomas[2]*

[1]Research Institute of Unconventional Petroleum and Renewable Energy, China University of Petroleum (East China), Qingdao, Shandong 266580, P. R. China

E-mail: zhaoxuebo@upc.edu.cn

[2]Wolfson Northern Carbon Reduction Laboratories, School of Chemical Engineering and Advanced Materials, Newcastle University, Newcastle upon Tyne, NE1 7RU, U.K.

E-mail: mark.thomas@ncl.ac.uk

[3]Qingdao Institute of Bioenergy and Bioprocess Technology, Chinese Academy of Sciences, Qingdao, Shandong 266101, P. R. China

[4]University of Chinese Academy of Sciences, Beijing 100049, P. R. China

[5] Present Address: School of Chemistry and Chemical Engineering, Qufu Normal University, Qufu, Shandong 273165, P. R. China

Contents

S1. Synthetic, Spectroscopic and Analytical Information

1.1. Materials used

All reagents and solvents were commercially available and used without further purification. 5-aminoisophthalic acid (98%), 1,2,4,5-tetramethylbenzene (99%) and lanthanide(III) nitrate hexahydrate ($Ln(NO_3)_3 \cdot 6H_2O$, where Ln = La, Ce, Pr, Nd, Sm, Eu, Gd, Tb, Dy, Er) (99.9%) were purchased from Aladdin Industrial Inc. Methanol (≥ 99.5%), ethanol (≥ 99.7%), acetonitrile (≥ 99.0%), diethyl ether (≥ 99.7%), dichloromethane (≥ 99.5%), chloroform (≥ 99.0%) and 1,2-dichloroethane (≥ 99.0%), tetrahydrofuran (≥ 99.0%), N,N-dimethylacetamide (DMA) (≥ 99.0%), sulfuric acid (95.0% ~ 98.0%), hydrochloride acid (36.0%), nitric acid (65.0%), sodium hydroxide (≥ 96.0%), sodium sulfate (anhydrous, ≥ 99.0%), sodium carbonate anhydrous (≥ 99.8%), potassium carbonate anhydrous (≥ 99.0%) and paraformaldehyde (≥ 95.0%) were purchased from Sinopharm Chemical Reagent Co., Ltd. Hydrobromic acid (33 wt% solution in acetic acid) was purchased from J&K Scientific Ltd. High purity (99.999%) gases of nitrogen, oxygen, hydrogen, methane and carbon dioxide and solid carbon dioxide were provided by Qingdao Heli Gas Co., Ltd, China.

1.2 Ligand Synthetic Scheme

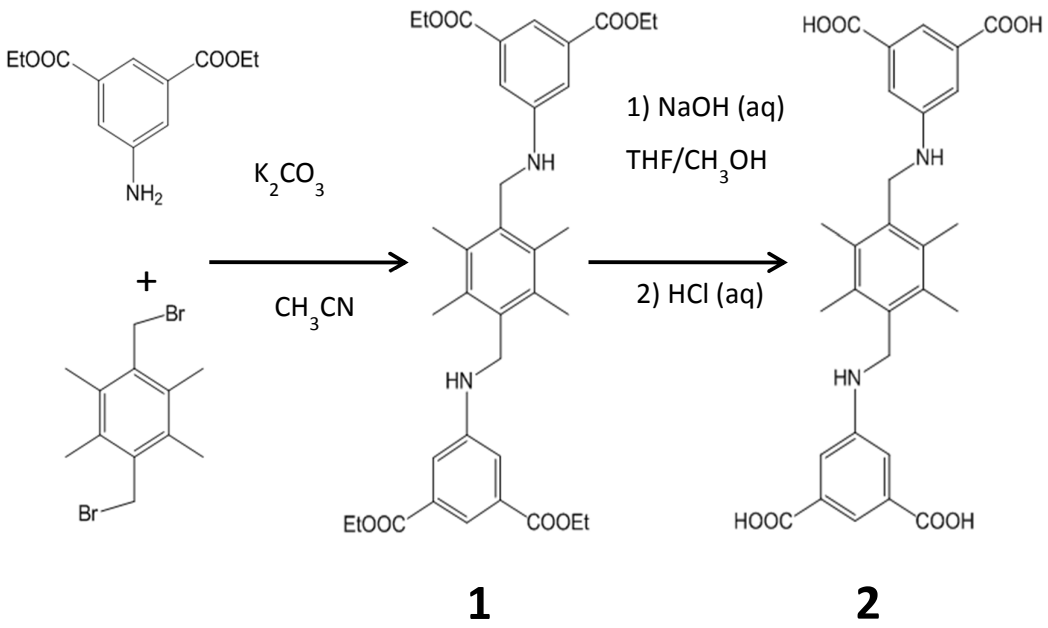

Scheme S1. Synthesis of the tetracarboxylate ligand 2 (H_4L).

1.3 Ligand and MOF Characterization

1.3.1 Spectroscopic Data for the Ligand and Precursors

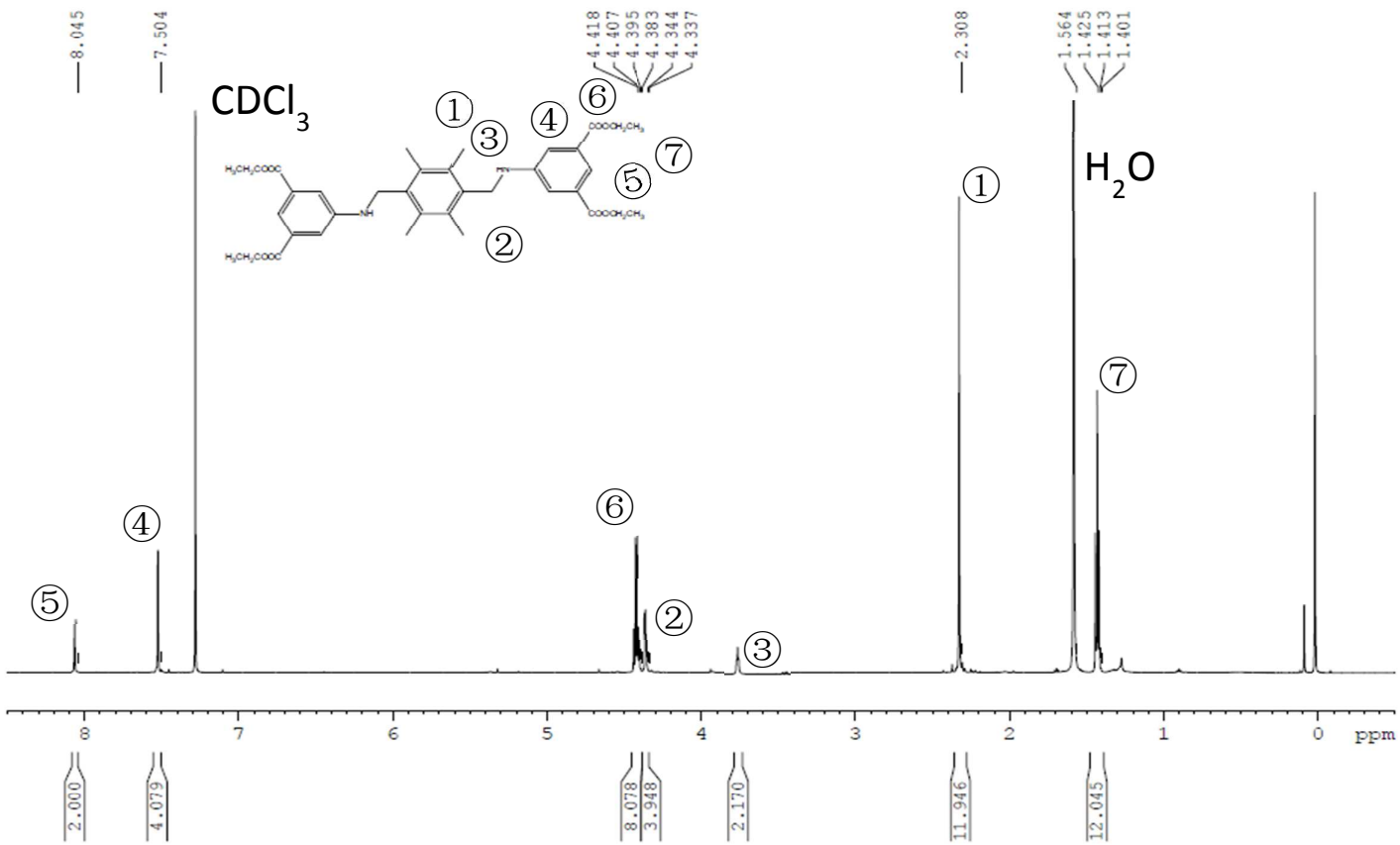

Figure S1. ^{1}H NMR spectrum of **1** (***tetraethyl 5,5'-(2,3,5,6-tetramethyl-1,4-phenylene)bis(methylene) bis(azanediyl) diisophthalate.***) and peak assignments.

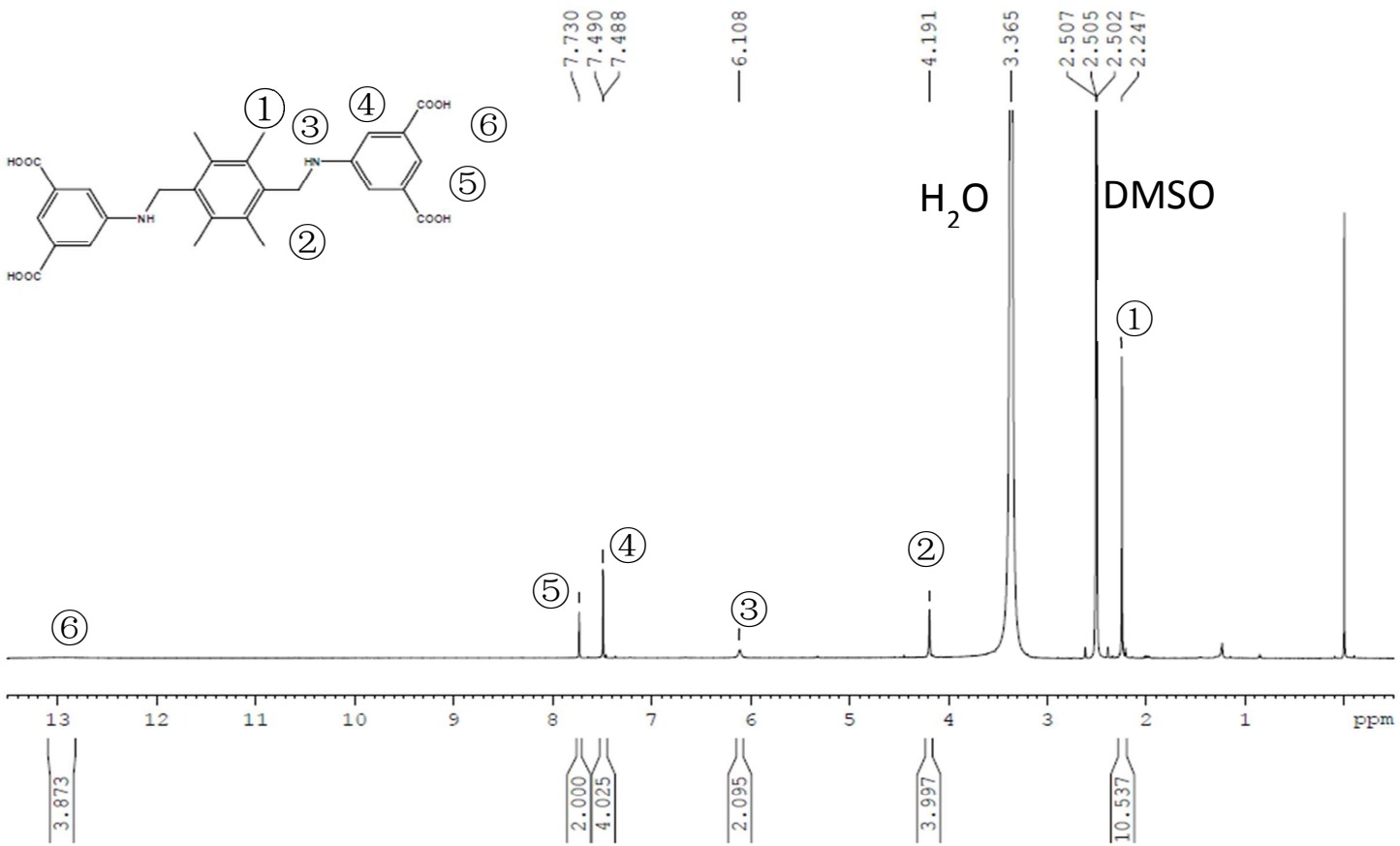

Figure S2. ^{1}H NMR spectrum of **2 (*5,5'-(2,3,5,6-tetramethyl-1,4-phenylene)bis(methylene) bis (azanediyl) diisophthalic acid (H_4L)*)** and peak assignments.

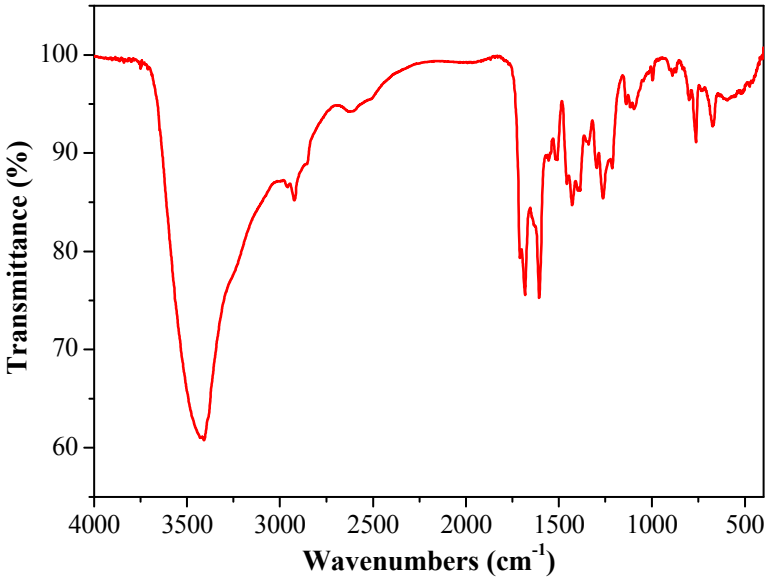

Figure S3. IR spectrum of ligand H_4L.

1.3.2. Characterization Data for the Ln-MOFs

[La(HL)(DMA)$_2$]·DMA·2H$_2$O: Yield: 0.050 g (51%) based on H_4L. Elemental analysis for $C_{40}H_{58}N_5LaO_{14}$ (M_r = 953.80) (%): calcd: H 5.92, C 50.37, N 7.34; found: H 5.52, C 49.79, N 7.33. IR data (KBr, cm^{-1}): 3428 (b), 2920 (w), 2850 (w), 1609 (s), 1540 (s), 1424 (m), 1384 (m), 1283 (w), 1256 (w), 1144 (w), 1097 (w), 1056(w), 1024 (w), 780 (m), 723 (w), 673 (w), 596 (w).

[**Ce(HL)(DMA)$_2$]·DMA·2H$_2$O:** Yield: 0.040 g (41%) based on H_4L. Elemental analysis for $C_{40}H_{58}N_5O_{14}Pr$ (M_r = 955.01) (%): calcd: H 5.91, C 50.31, N 7.33; found: H 5.68, C 50.18, N 7.25.

[Pr(HL)(DMA)$_2$]·DMA·2H$_2$O: Yield: 0.040 g (41%) based on H_4L. Elemental analysis for $C_{40}H_{58}N_5O_{14}Pr$ (M_r = 955.81) (%): calcd: H 5.91, C 50.26, N 7.33; found: H 5.90, C 50.28, N 7.22.

[Nd(HL)(DMA)$_2$]·DMA·2H$_2$O: Yield: 0.048 g (49%) based on H_4L. Elemental analysis for $C_{40}H_{58}N_5O_{14}Nd$ (M_r = 959.14) (%): calcd: H 5.88, C 50.09, N 7.30; found: H 5.85, C 49.96, N 7.08.

[Sm(HL)(DMA)$_2$]·DMA·2H$_2$O: Yield: 0.039 g (42%) based on H_4L. Elemental analysis for $C_{40}H_{58}N_5SmO_{14}$ (M_r = 965.26) (%): calcd: H 5.85, C 49.77, N 7.26; found: H 5.51, C 48.75, N 7.12. IR data (KBr, cm^{-1}): 3436 (b), 2917 (w), 2847 (w), 1617 (s), 1537 (s), 1432 (m), 1382 (m), 1283 (w), 1258 (w), 1147 (w), 1099 (w), 1052 (w), 1024 (w), 780 (m), 723 (w), 666 (w), 596 (w).

[Eu(HL)(DMA)$_2$]·DMA·2H$_2$O: Yield: 0.050 g (53%) based on H_4L. Elemental analysis for $C_{40}H_{58}N_5O_{14}Eu$ (M_r = 966.96) (%): calcd: H 5.84, C 49.69, N 7.24; found: H 5.84, C 48.75, N 7.23.

[Gd(HL)(DMA)$_2$]·DMA·2H$_2$O: Yield: 0.042 g (45%) based on H_4L. Elemental analysis for $C_{40}H_{58}N_5O_{14}Gd$ (M_r = 972.15) (%): calcd: H 5.81, C 49.42, N 7.20; found: H 5.49, C 49.46, N 6.89.

[Tb(HL)(DMA)$_2$]·DMA·2H$_2$O: Yield: 0.043 g (45%) based on H_4L. Elemental analysis for $C_{40}H_{58}N_5O_{14}Tb$ (M_r = 973.82) (%): calcd: H 5.80, C 49.33, N 7.19; found: H 5.64, C 49.52, N 7.02.

[Dy(HL)(DMA)$_2$]·DMA·2H$_2$O: Yield: 0.042 g (44%) based on H_4L. Elemental analysis for $C_{40}H_{58}N_5O_{14}Dy$ (M_r = 977.40) (%): calcd: H 5.78, C 49.15, N 7.17; found: H 5.58, C 49.42, N 7.12.

[Er(HL)(DMA)$_2$]·DMA·2H$_2$O: Yield: 0.045 g (45%) based on H_4L. Elemental analysis for $C_{40}H_{58}N_5O_{14}Nd$ (M_r = 982.16) (%): calcd: H 5.75, C 48.92, N 7.13; found: H 5.31, C 48.82, N 7.00.

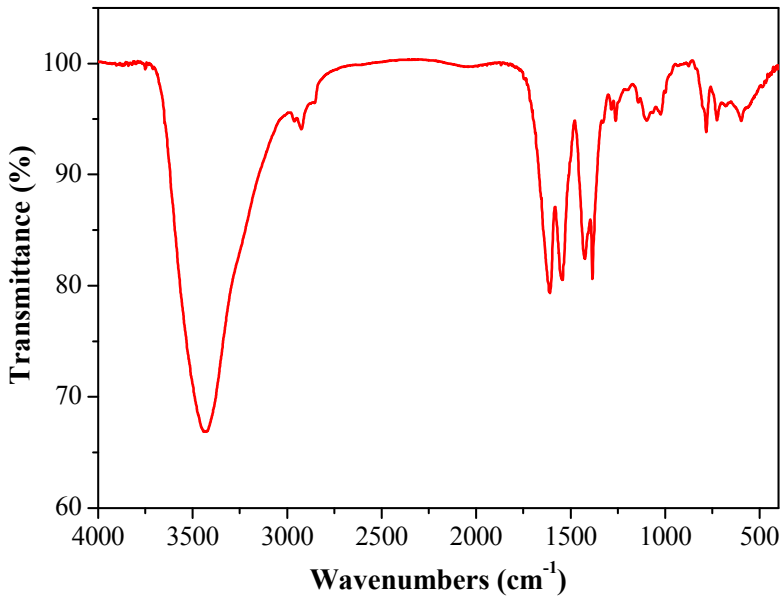

Figure S4. IR spectrum of *trans*-[La(HL)(DMA)$_2$]·DMA·2H$_2$O.

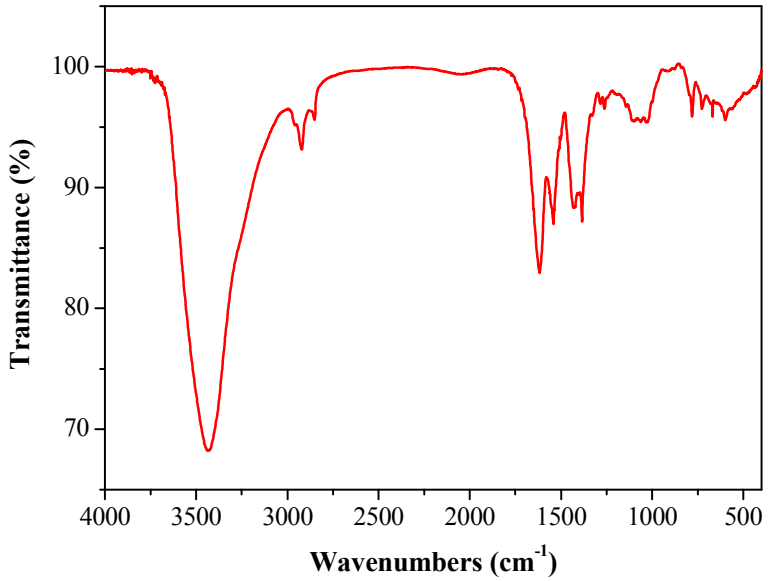

Figure S5. IR spectrum of *trans*-[Sm(HL)(DMA)$_2$]·DMA·2H$_2$O.

S2. X-ray Diffraction Studies and Additional Crystal Structure Information

2.1 Powder X-Ray Diffraction (PXRD) Profiles of $[Ln(HL)(DMA)_2]\cdot DMA\cdot 2H_2O$ where Ln = La, Ce, Pr, Nd, Sm, Eu, Gd, Tb, Dy and Er.

(a)

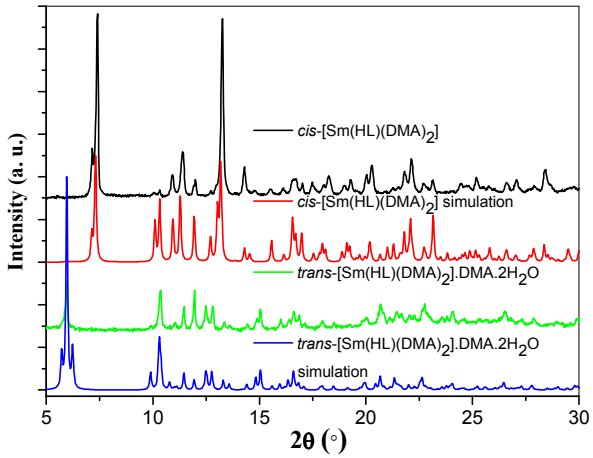

(b)

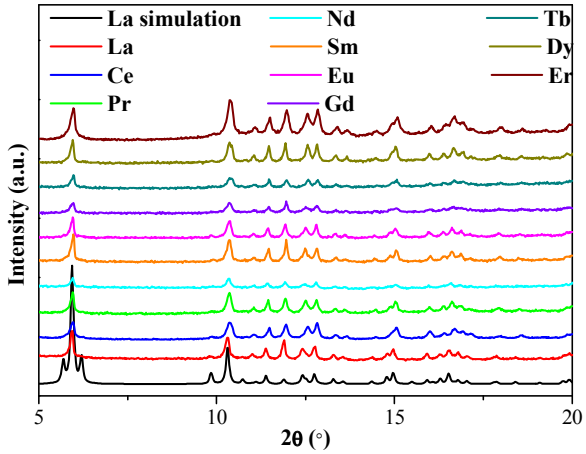

Figure S6. (a) PXRD simulated and experimental profiles for *trans*-$[Sm(HL)(DMA)_2]\cdot DMA\cdot 2H_2O$ and *cis*-$[Sm(HL)(DMA)_2]$(activated), (b) PXRD profiles for the series of iso-structural lanthanide-based metal-organic frameworks (*trans*-$[Ln(HL)(DMA)_2]\cdot DMA\cdot 2H_2O$) where Ln = La, Ce, Pr, Nd, Sm, Eu, Gd, Tb, Dy and Er.

2.2 Single Crystal X-ray Diffraction

Table S1. Comparison of Unit Cell Parameters for *trans*-[La(HL)(DMA)$_2$]·DMA·2H$_2$O *trans*-[Sm(HL)(DMA)$_2$]·DMA·2H$_2$O and *trans*-[Tb(HL)(DMA)$_2$]·DMA·2H$_2$O at 293 K obtained by single-crystal X-ray diffraction.

Identification Code	*trans*-[La(HL)(DMA)$_2$]·DMA·2H$_2$O	*trans*-[Sm(HL)(DMA)$_2$]·DMA·2H$_2$O	*trans*-[Tb(HL)(DMA)$_2$]·DMA·2H$_2$O*
Empirical formula	$C_{36}H_{43}N_4O_{10}La$	$C_{36}H_{43}N_4O_{10}Sm$	$C_{36}H_{43}N_4O_{10}Tb$
Formula weight	830.65	842.09	850.66
Crystal system	Monoclinic	Monoclinic	Monoclinic
space group	C2/c	C2/c	C2/c
a/Å	32.985(7)	32.84(3)	32.85(5)
b/Å	8.9901(19)	8.998(8)	8.897(14)
c/Å	34.432(7)	34.21(3)	34.21(6)
α/deg.	90.00	90.00	90.00
β/deg.	115.591(2)	115.564(11)	116.49(1)
γ/deg.	90.00	90.00	90.00
V/Å^3	9209(3)	9119(14)	8940(60)

*Only unit cell parameters were collected. Single crystal data were collected for *trans*-[Sm(HL)(DMA)$_2$]·DMA·2H$_2$O and *trans*-[La(HL)(DMA)$_2$]·DMA·2H$_2$O.The emprical formula excludes solvent molecules

Table S2. Crystal Data and Structure Refinement for *trans*-[Sm(HL)(DMA)$_2$]·DMA·2H$_2$O and *cis*-[Sm(HL)(DMA)$_2$] at 293 K.

Identification code	*trans*-[Sm(HL)(DMA)$_2$] ·DMA·2H$_2$O	*cis*-[Sm(HL)(DMA)$_2$]
Empirical formula	$C_{36}H_{43}N_4O_{10}Sm$	$C_{36}H_{43}N_4O_{10}Sm$
Formula weight	842.09	842.09
Temperature/K	293(2)	293(2)
Wavelength/Å	0.71073	0.71073
Crystal system	Monoclinic	Monoclinic
space group	C2/c	C2/c
a/Å	32.84(3)	32.14(2)
b/Å	8.998(8)	9.156(6)
c/Å	34.21(3)	26.864(18)
α/deg.	90.00	90.00
β/deg.	115.564(11)	112.859(7)
γ/deg.	90.00	90.00
V/Å^3	9119(14)	7285(8)
Z	8	8
D_{calcd} /g ·cm^{-3}	1.227	1.536
Absorption coefficient/mm^{-1}	1.337	1.674
F(000)	3432	3432
Crystal size/mm	0.20 x 0.02 x 0.02	0.20 x 0.02 x 0.02
θ range for data collection	2.28 to 25.00 °.	1.38 to 25.00 °.
Limiting indices	-38 ≤ h ≤ 38, -10 ≤ k ≤10, -40 ≤l ≤38	-38 ≤h ≤ 36, -10 ≤ k ≤10, -31 ≤l ≤31
Reflections collected / unique	22613 / 7876 [R(int) = 0.1331]	21958 / 6376 [R(int) = 0.0902]
Completeness to theta = 25.00	98.0 %	99.7 %
Absorption correction	Semi-empirical from equivalents	Semi-empirical from equivalents
Max. and min. transmission	0.9737 and 0.7758	0.8504 and 0.7307
Refinement method	Full-matrix least-squares on F^2	Full-matrix least-squares on F^2
Data / restraints / parameters	7876 / 652 / 429	6376 / 15 / 433
Goodness-of-fit on F^2	1.049	1.051
R_1^a , wR_2^b [I>2σ(I)]	0.0639 , 0.1432	0.0625 , 0.1434
R_1^a , wR_2^b (all data)	0.1228 , 0.1713	0.1113 , 0.1565
Largest diff. peak and hole /e Å^{-3}	1.458 , -1.761	1.058 , -1.231

The emprical formula excludes solvent molecules for *trans*-[Sm(HL)(DMA)$_2$]·DMA·2H$_2$O

Table S3. Crystal Data and Structure Refinement for *trans*-[Sm(HL)(DMA)$_2$]·2.8 CH_2Cl_2 at 173 K.

Identification code	*trans*-[Sm(HL)(DMA)$_2$]·2.8CH_2Cl_2 (173 K)
Empirical formula	$C_{36}H_{43}N_4O_{10}Sm$
Formula weight	842.09
Temperature/K	173(2)
Wavelength/Å	0.71073
Crystal system	Monoclinic
space group	C2/c
a/Å	32.599(5)
b/Å	8.8449(14)
c/Å	34.246(8)
α/deg.	90.00
β/deg.	116.457(2)
γ/deg.	90.00
V/Å^3	8840(3) Å^3
Z	8
D_{calcd} /g ·cm^{-3}	1.265
Absorption coefficient/mm^{-1}	1.380
F(000)	3432
Crystal size/mm	0.20 x 0.02 x 0.02
θ range for data collection	1.33 to 25.00 °.
Limiting indices	$-38 \leq h \leq 38$, $-10 \leq k \leq 10$, $-33 \leq l \leq 40$
Reflections collected / unique	29796 / 7782 [R(int) = 0.0933]
Completeness to theta = 25.00	100.0 %
Absorption correction	Semi-empirical from equivalents
Max. and min. transmission	0.9096 and 0.7699
Refinement method	Full-matrix least-squares on F^2
Data / restraints / parameters	7782 / 0 / 459
Goodness-of-fit on F^2	1.048
R_1^a , wR_2^b [I>2σ(I)]	0.0507 , 0.0929
R_1^a , wR_2^b (all data)	0.0887 , 0.0991
Largest diff. peak and hole /e Å^{-3}	0.656 , -1.138

The emprical formula excludes solvent guest molecules

Table S4. Crystal Data and Structure Refinement for *trans*-[La(HL)(DMA)$_2$]·DMA·2H$_2$O at 293 K.

Identification code	*trans*-[La(HL)(DMA)$_2$]·DMA·2H$_2$O
Empirical formula	$C_{36}H_{43}N_4O_{10}La$
Formula weight	830.65
Temperature/K	293(2)
Wavelength/Å	0.71073
Crystal system	Monoclinic
space group	C2/c
a/Å	32.985(7)
b/Å	8.9901(19)
c/Å	34.432(7)
α/deg.	90.00
β/deg.	115.591(2)
γ/deg.	90.00
V/Å^3	9209(3)
Z	8
D_{calcd} /g ·cm^{-3}	1.197
Absorption coefficient/mm^{-1}	0.977
F(000)	3392
Crystal size/mm	0.20 x 0.02 x 0.02
θ range for data collection	2.27 to 25.00 °.
Limiting indices	$-33 \leq h \leq 39$, $-10 \leq k \leq 10$, $-40 \leq l \leq 40$
Reflections collected / unique	25159 / 8103 [R(int) = 0.0593]
Completeness to theta = 25.00	99.8 %
Absorption correction	Semi-empirical from equivalents
Max. and min. transmission	0.9086 and 0.8286
Refinement method	Full-matrix least-squares on F^2
Data / restraints / parameters	8103 / 682 / 423
Goodness-of-fit on F^2	1.127
R_1^a , wR_2^b [I>2σ(I)]	0.0554 , 0.1480
R_1^a , wR_2^b (all data)	0.0720 , 0.1546
Largest diff. peak and hole /e Å^{-3}	1.530 , -1.528

The emprical formula excludes solvent molecules for *trans*-[La(HL)(DMA)$_2$]·DMA·2H$_2$O

2.3 Additional Crystal Structure Descriptions

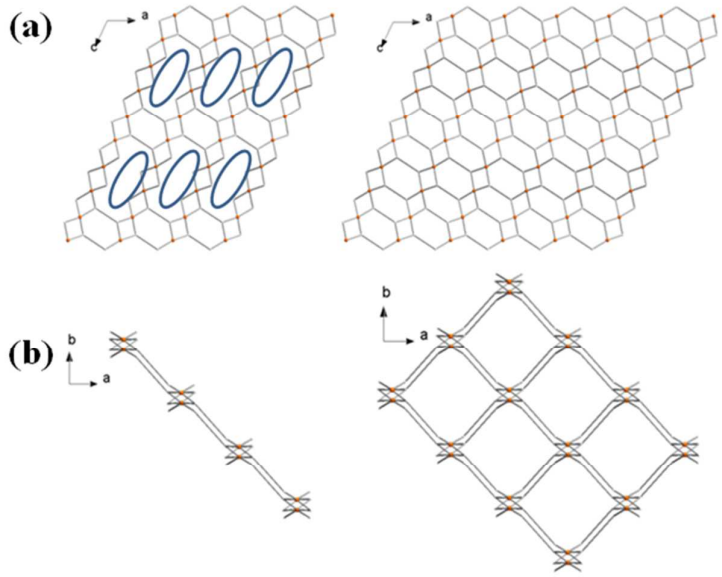

Figure S7. Simplified views of the single network of *trans*-[Sm(HL)(DMA)$_2$] ·DMA·2H$_2$O. The single 2D layer and 3D network along (a) ***b***- and (b) ***c***-axis.

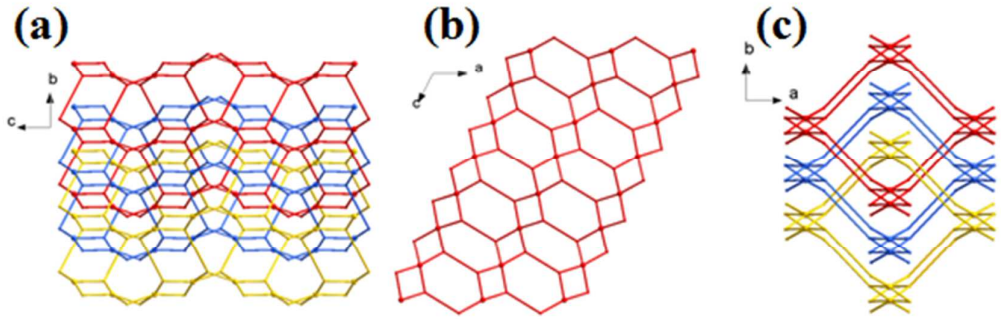

Figure S8. Simplified view of the 3-fold interpenetration framework structure of *trans*-[Sm(HL)(DMA)$_2$]·DMA·2H$_2$O with the different networks shown in red, blue and yellow along (a) ***a***-axis, (b) ***b***- axis and (c) ***c***-axis.

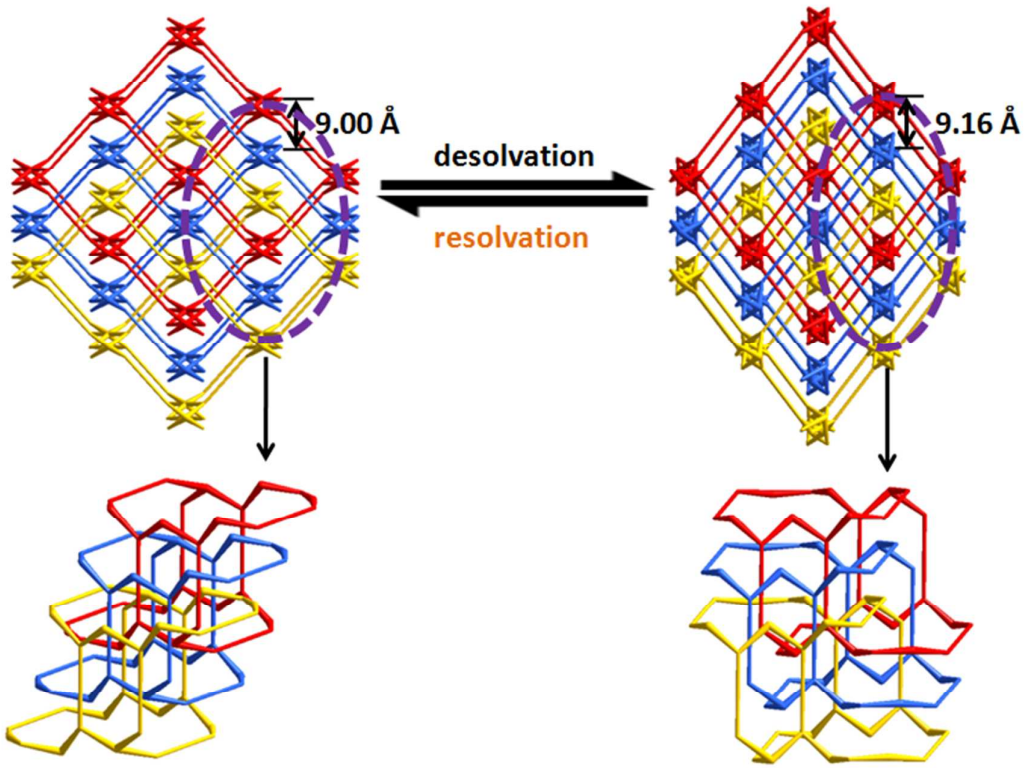

Figure S9. Simplified views of the change of interpenetration details on desolvation and resolvation between ·*trans*-[Sm(HL)(DMA)$_2$]·DMA·2H$_2$O and *cis*-[Sm(HL)(DMA)$_2$].

(a) *trans*-[Sm(HL)(DMA)$_2$]·DMA·2H$_2$O

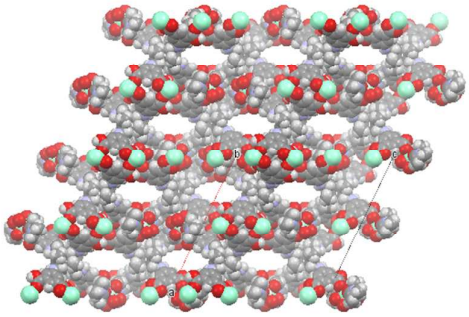

(b) *trans*-[Sm(HL)(DMA)$_2$]·2.8CH$_2$Cl$_2$ (173 K)

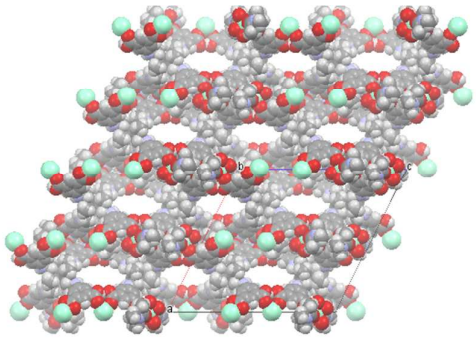

(c) *trans*-[La(HL)(DMA)$_2$]·DMA·2H$_2$O

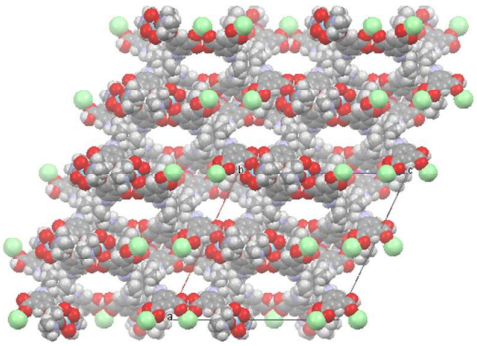

(d) *cis*-[Sm(HL)(DMA)$_2$]

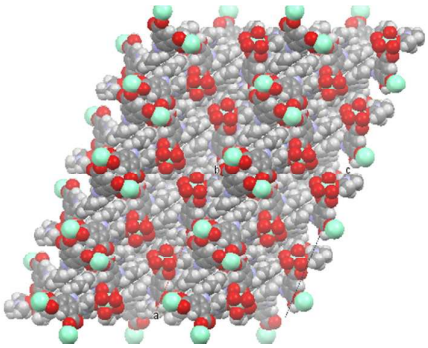

Figure S10 Crystallographic packing diagrams viewed along the ***b***-axis of (a) *trans*-[Sm(HL)(DMA)$_2$]·DMA·2H$_2$O, (b) *trans*-[Sm(HL)(DMA)$_2$]·2.8CH$_2$Cl$_2$, (c) *trans*-[La(HL)(DMA)$_2$]·DMA·2H$_2$O and (d) *cis*-[Sm(HL)(DMA)$_2$]

(a) ***trans*-[Sm(HL)(DMA)$_2$]·DMA·2H$_2$O**

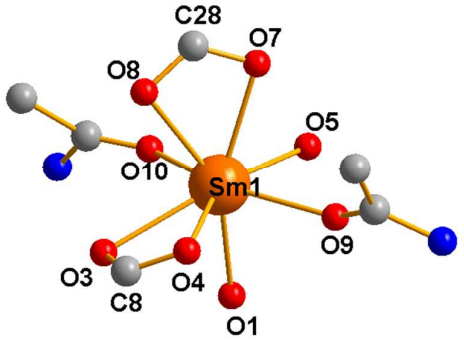

Sm-O bond lengths (Å)
DMA: Sm-O9 = 2.406(8), Sm-O10 = 2.303(8)
Bidentate: Sm-O3 = 2.501(6), Sm-O4 = 2.438(6), Sm-O7 = 2.453(8), Sm-O8 = 2.482(8).
Mondentate: Sm-O1 = 2.343(8), Sm-O5 = 2.432(5)

(b) ***trans*-[Sm(HL)(DMA)$_2$]·2.8CH$_2$Cl$_2$ (173 K)**

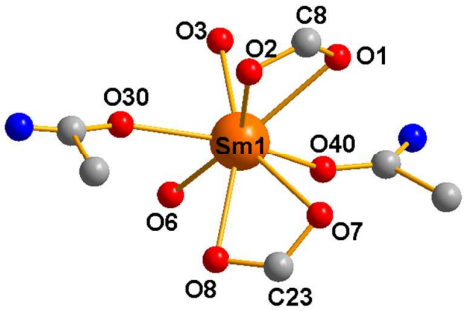

Bond lengths(Å)
DMA: Sm-O30 = 2.382(5), Sm-O40 = 2.315(5)
Bidentate: Sm-O1 = 2.510(4), Sm-O2 = 2.431(4), Sm-O7 =2.437(5), Sm-O8 = 2.543(5)
Monodentate: Sm-O3 = 2.345(6), Sm-O6 = 2.406(3)

(c) ***trans*-[La(HL)(DMA)$_2$]·DMA·2H$_2$O**

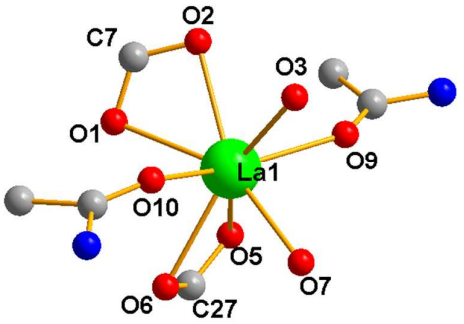

La-O bond lengths (Å)
DMA: La-O9 = 2.471(5), La-O10 = 2.405(5)
Bidentate: La-O1=2.552(5), La-O2 =2.525(6), La-O5 = 2.507(4) , La-O6 = 2.588(4)
Mondentate: La-O3 =2.505(3), La-O7 = 2.453(6)

(d) <u>*cis*-[Sm(HL)(DMA)$_2$]</u>

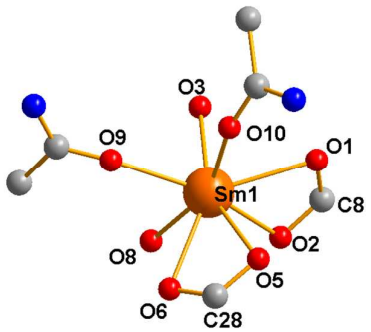

Sm-O bond lengths (Å)
DMA: Sm-O9 = 2.384(9), Sm-O10 = 2.320(8)
Bidentate: Sm-O5 = 2.414(8), Sm-O6 = 2.489(6), Sm-O1 = 2.523(5), Sm-O2 = 2.414(8).
Mondentate: Sm-O3 =2.345(7) , Sm-O8 = 2.408(7)

Figure S11 Metal oxygen bond lengths (a) *trans*-[Sm(HL)(DMA)$_2$]·DMA·2H_2O, (b) *trans*-[Sm(HL)(DMA)$_2$]·2.8CH_2Cl_2 (173 K), (c) *trans*-[La(HL)(DMA)$_2$]·DMA·2H_2O and (d) *cis*-[Sm(HL)(DMA)$_2$].

2.4 Heat treatment studies

(a)

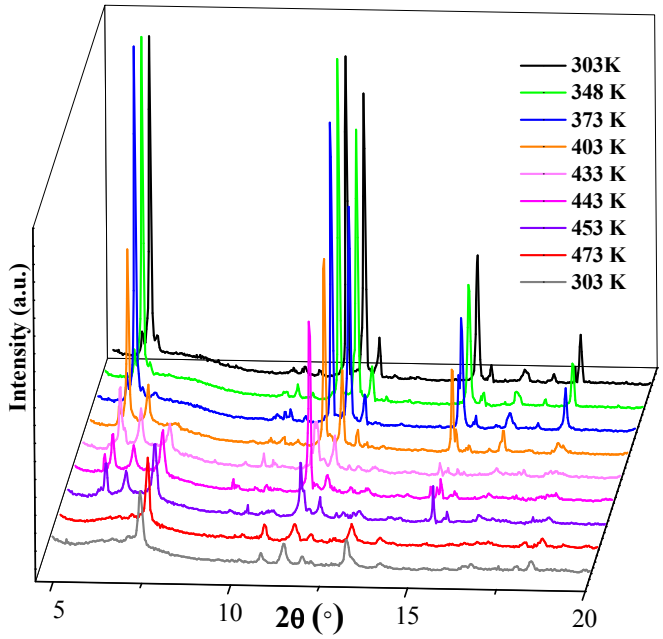

(b)

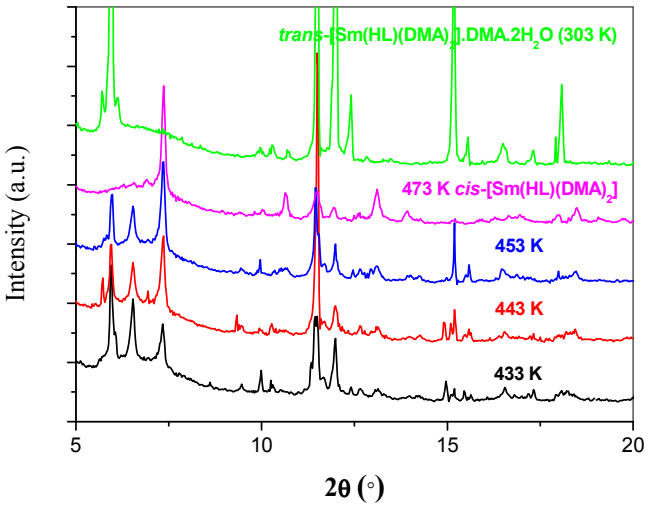

Figure S12. (a) The development of the PXRD profiles of *trans*-[Sm(HL)(DMA)$_2$]·DMA·2H$_2$O during desolvation by heat treatment from 303 to 473 K and return to 303 K at atmospheric pressure, and (b) Comparison of PXRD profiles for *trans*-[Sm(HL)(DMA)$_2$]·DMA·2H$_2$O (303 K) and heat treated samples to 433, 443, 453 and 473 K at atmospheric pressure.

2.5 Guest Exchange Studies

Table S5. Guest exchanged samples and their corresponding framework structures.

Sample	**Framework Structure**	**Description**
trans-[Sm(HL)(DMA)$_2$]·DMA·2H$_2$O	*trans* DMA coordination*	as synthesized
cis-[Sm(HL)(DMA)$_2$]	*cis* DMA coordination*	*trans*-[Sm(HL)(DMA)$_2$]·DMA·2H$_2$O activated by heating to 200°C
cis-[Sm(HL)(DMA)$_2$]·DMA	*trans* DMA coordination^P	*cis*-Sm(HL)(DMA)$_2$ soaked in DMA
cis-[Sm(HL)(DMA)$_2$]·CH$_2$Cl$_2$-ad	intermediate phase^P	*cis*-Sm(HL)(DMA)$_2$ soaked in CH$_2$Cl$_2$ and air dried for 12h
cis-[Sm(HL)(DMA)$_2$]·CHCl$_3$-ad	intermediate phase^P	*cis*-Sm(HL)(DMA)$_2$ soaked in CHCl$_3$ and air dried for 12h
cis-[Sm(HL)(DMA)$_2$]·C$_2$H$_4$Cl$_2$-ad	intermediate phase^P	*cis*-Sm(HL)(DMA)$_2$ soaked in C$_2$H$_4$Cl$_2$ and air dried for 12h
trans-[Sm(HL)(DMA)$_2$]·2.8CH$_2$Cl$_2$ (173K)	*trans* DMA coordination*	*trans*-[Sm(HL)(DMA)$_2$]·DMA·2H$_2$O solvent exchanged in CH$_2$Cl$_2$ and cooled to 173 K to avoid solvent loss during structure determination
trans-[Sm(HL)(DMA)$_2$]·CH$_2$Cl$_2$	Trans + intermediate phase^P	*trans*-[Sm(HL)(DMA)$_2$]·DMA·2H$_2$O solvent exchanged in CH$_2$Cl$_2$
cis-[Sm(HL)(DMA)$_2$]·CH$_2$Cl$_2$	Trans + intermediate phase^P	*cis*-Sm(HL)(DMA)$_2$ soaked in CH$_2$Cl$_2$
trans-[Sm(HL)(DMA)$_2$]·CH$_2$Cl$_2$-ad	intermediate phase^P	*trans*-[Sm(HL)(DMA)$_2$]·DMA·2H$_2$O solvent exchanged in CH$_2$Cl$_2$ and air dried for 12h
trans-[Ln(HL)(DMA)$_2$]·DMA·2H$_2$O	*trans* DMA coordination*	as synthesized [Ln(HL)(DMA)$_2$]·DMA·2H$_2$O, Ln = La, Tb etc.

* - single crystal structure. The single crystal *trans*-[Sm(HL)(DMA)$_2$]·2.8CH$_2$Cl$_2$ structure at 173 K, where solvent loss was minimal, was very similar to *trans*-[Sm(HL)(DMA)$_2$]·DMA·2H$_2$O. ^{P} – structure characterization from PXRD profiles.

(a)

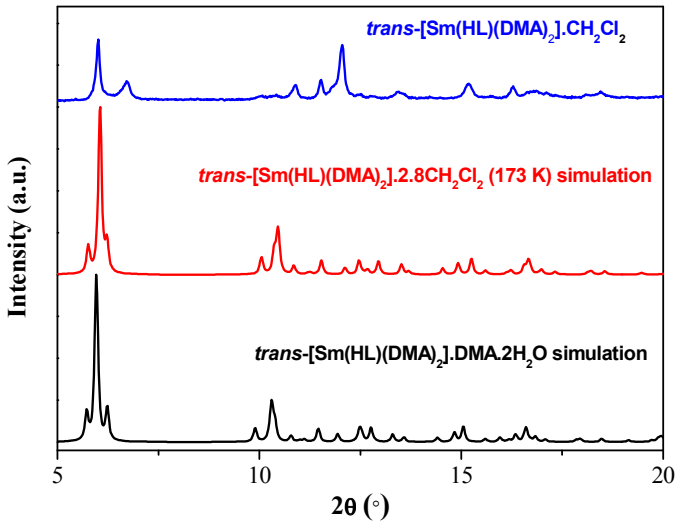
trans-[Sm(HL)(DMA)2].CH2Cl2
trans-[Sm(HL)(DMA)2].2.8CH2Cl2 (173 K) simulation
trans-[Sm(HL)(DMA)2].DMA.2H2O simulation
Intensity (a.u.)
5
10
15
20
2θ (◦)

(b)

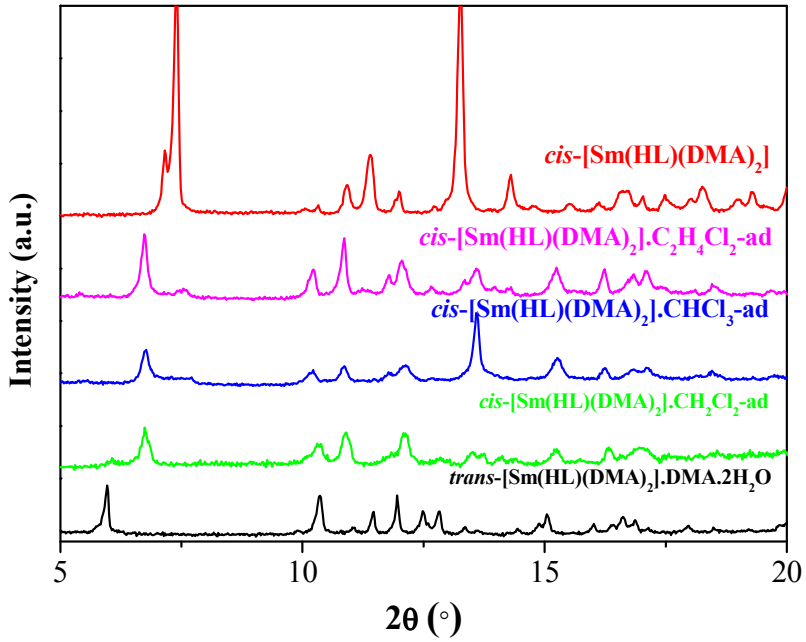
cis-[Sm(HL)(DMA)2]
cis-[Sm(HL)(DMA)2].C2H4Cl2-ad
cis-[Sm(HL)(DMA)2].CHCl3-ad
cis-[Sm(HL)(DMA)2].CH2Cl2-ad
trans-[Sm(HL)(DMA)2].DMA.2H2O
Intensity (a.u.)
5
10
15
20
2θ (◦)

(c)

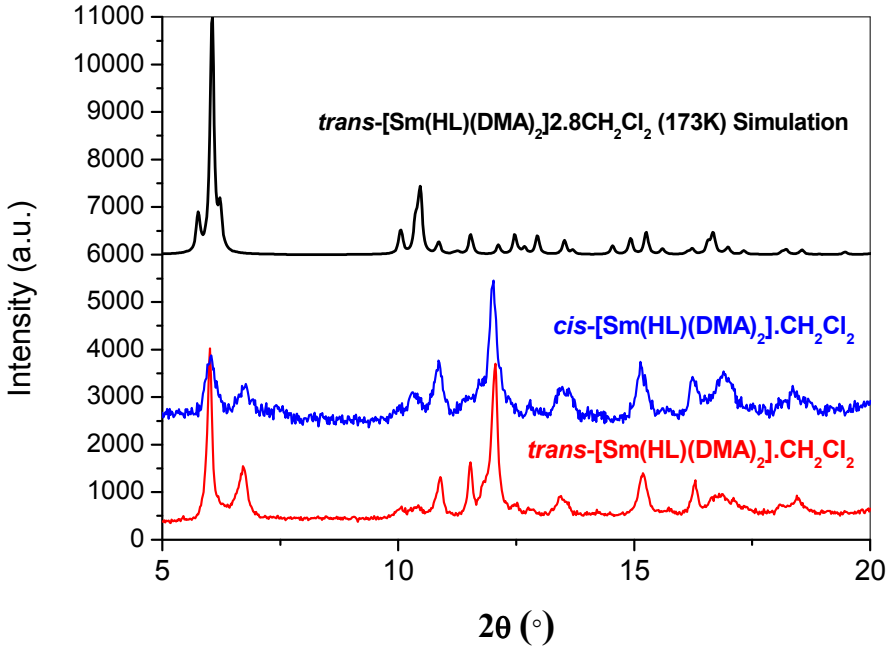
11000
10000
9000
8000
7000
6000
5000
4000
3000
2000
1000
0
Intensity (a.u.)
trans-[Sm(HL)(DMA)2]2.8CH2Cl2 (173K) Simulation
cis-[Sm(HL)(DMA)2].CH2Cl2
trans-[Sm(HL)(DMA)2].CH2Cl2
5
10
15
20
2θ (◦)

(d)

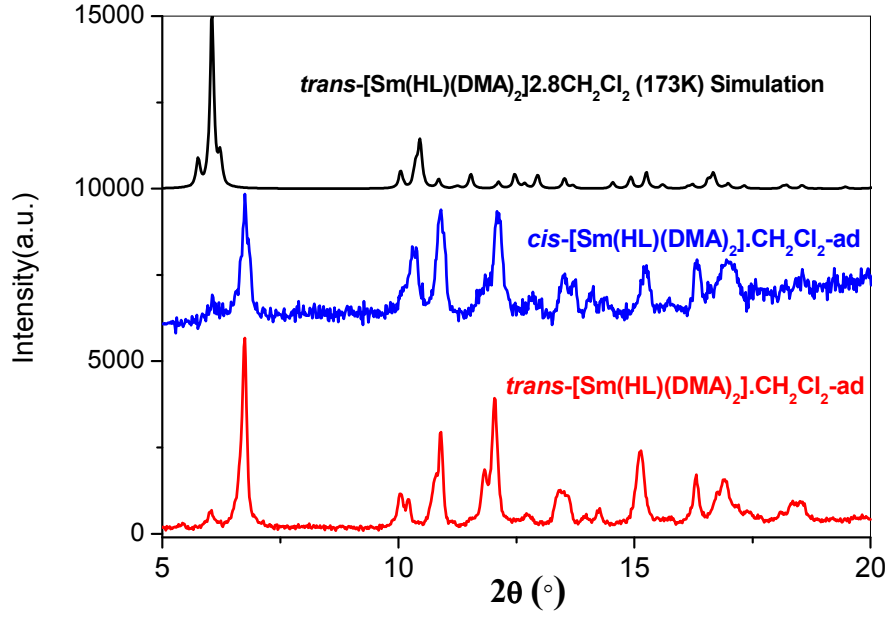
15000
10000
5000
0
Intensity(a.u.)
trans-[Sm(HL)(DMA)2]2.8CH2Cl2 (173K) Simulation
cis-[Sm(HL)(DMA)2].CH2Cl2-ad
trans-[Sm(HL)(DMA)2].CH2Cl2-ad
5
10
15
20
2θ (◦)

(e)

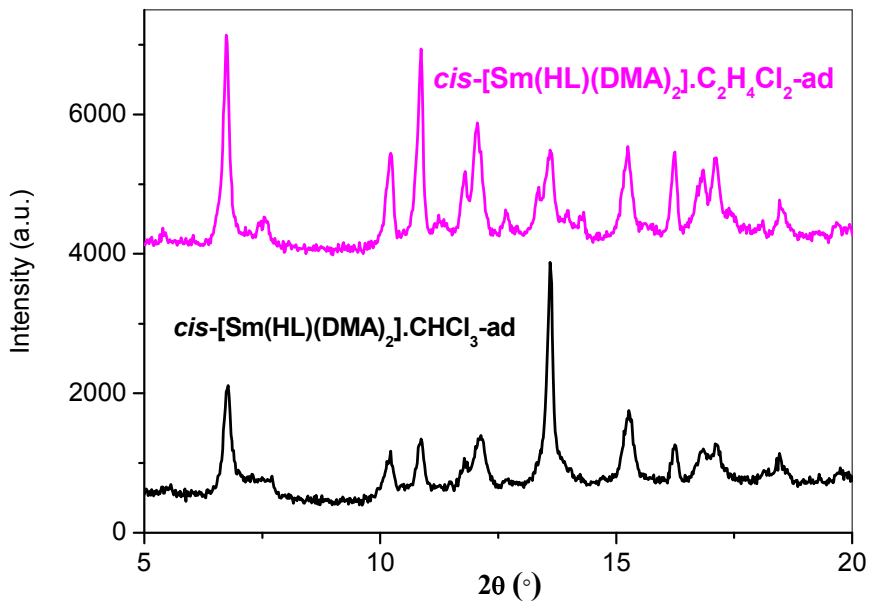
cis-[Sm(HL)(DMA)2].C2H4Cl2-ad
cis-[Sm(HL)(DMA)2].CHCl3-ad
Intensity (a.u.)
6000
4000
2000
0
5
10
15
20
2θ (◦)

(f)

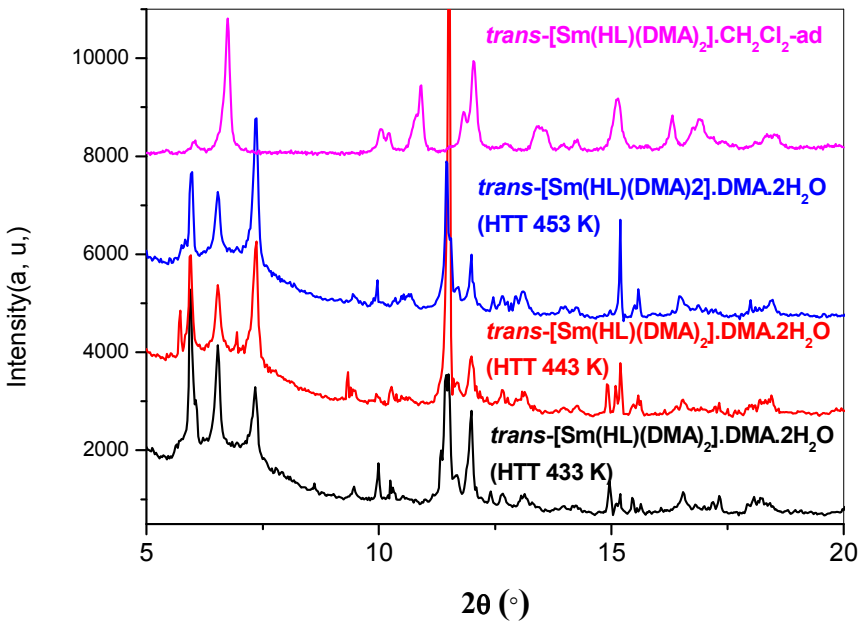
trans-[Sm(HL)(DMA)2].CH2Cl2-ad
trans-[Sm(HL)(DMA)2].DMA.2H2O
(HTT 453 K)
trans-[Sm(HL)(DMA)2].DMA.2H2O
(HTT 443 K)
trans-[Sm(HL)(DMA)2].DMA.2H2O
(HTT 433 K)
Intensity(a, u,)
10000
8000
6000
4000
2000
5
10
15
20
2θ (◦)

Figure S13. Comparison of PXRD profiles for guest-exchange studies (a) PXRD simulated profiles for *trans*-[Sm(HL)(DMA)$_2$]·DMA·2H$_2$O and *trans*-[Sm(HL)(DMA)$_2$]·2.8CH$_2$Cl$_2$, and experimental *trans*-[Sm(HL)(DMA)$_2$]·CH$_2$Cl$_2$ profile; (b) *trans*-[Sm(HL)(DMA)$_2$]·DMA·2H$_2$O, *cis*-[Sm(HL)(DMA)$_2$], *cis*-[Sm(HL)(DMA)$_2$]·CH$_2$Cl$_2$-ad, *cis*-[Sm(HL)(DMA)$_2$]·CHCl$_3$-ad and *cis*-[Sm(HL)(DMA)$_2$]·C$_2$H$_4$Cl$_2$-ad; (c) *trans*-[Sm(HL)(DMA)$_2$]·2.8CH$_2$Cl$_2$ (173 K) computer simulation, *trans*-[Sm(HL)(DMA)$_2$]·CH$_2$Cl$_2$ and *cis*-[Sm(HL)(DMA)$_2$]·CH$_2$Cl$_2$; (d) *trans*-[Sm(HL)(DMA)$_2$]·2.8CH$_2$Cl$_2$ (173 K) computer simulation, *trans*-[Sm(HL)(DMA)$_2$]·CH$_2$Cl$_2$-ad and *cis*-[Sm(HL)(DMA)$_2$]·CH$_2$Cl$_2$-ad; (e) *cis*-[Sm(HL)(DMA)$_2$]·CHCl$_3$-ad and *cis*-[Sm(HL)(DMA)$_2$]·C$_2$H$_4$Cl$_2$-ad; (f) *trans*-[Sm(HL)(DMA)$_2$]·CH$_2$Cl$_2$-ad, *trans*-[Sm(HL)(DMA)$_2$]·DMA·2H$_2$O (HTT 433 K), *trans*-[Sm(HL)(DMA)$_2$]·DMA·2H$_2$O (HTT 443 K), *trans*-[Sm(HL)(DMA)$_2$]·DMA·2H$_2$O(HTT 453 K).
Intensities have been rescaled to avoid overlap of peaks. HTT = Heat Treatment Temperature

S3. Field Emission Scanning Electron Microscopy (FESEM) Studies

The FESEM images show the crystals of *trans*-[Sm(HL)(DMA)$_2$]·DMA·2H$_2$O to have the same rod-like morphology and non-uniform size with the width range of ca. 15 - 60 μm (Figure S14a,b). *cis*-[Sm(HL)(DMA)$_2$] retains its rod-like morphology structure after activation (Figure S14c,d). In contrast, gas adsorption resulted in fragmentation of the crystals (Figure S14e,f).

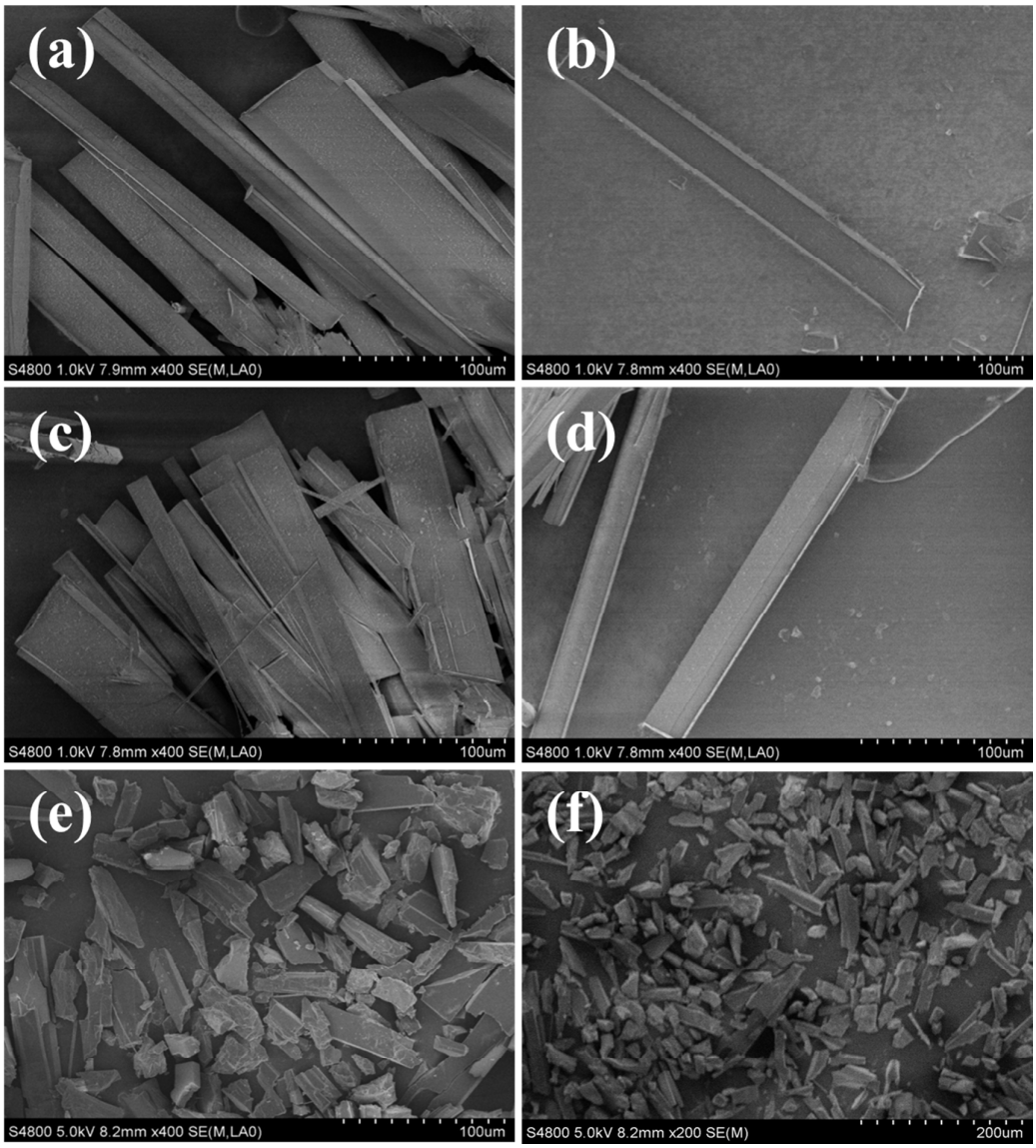

Figure S14. FESEM images of (a,b) *trans*-[Sm(HL)(DMA)$_2$]·DMA·2H$_2$O and (c,d) *cis*-[Sm(HL)(DMA)$_2$] before sorption and (e,f) *cis*-[Sm(HL)(DMA)$_2$] after CO_2 gas sorption measurements.

S4. Thermogravimetric Analysis (TGA)

The TGA profile of *trans*-[Sm(HL)(DMA)$_2$]·DMA·2H$_2$O shows a gradual weight loss between 30 and 165 °C and a rapid decrease from 165 to 205 °C on account of the loss of two lattice water molecules and one lattice DMA molecule per formula weight (found/calcd: 11.76/12.75%). Above 205 °C, *cis*-[Sm(HL)(DMA)$_2$] starts to decompose rapidly. Similarly, the TGA profiles of frameworks of *trans*-[Sm(HL)(DMA)$_2$]·CH$_2$Cl$_2$-ad and *cis*-[Sm(HL)(DMA)$_2$] show that they are stable to ~205 °C (see Figure S15). The TGA profiles of the other 'as-synthesized' *trans*-[Sm(HL)(DMA)$_2$]·DMA·2H$_2$O (Ln = La, Pr, Nd, Eu, Gd, Tb, Dy, Er) show similar thermal stability (see Figure S16).

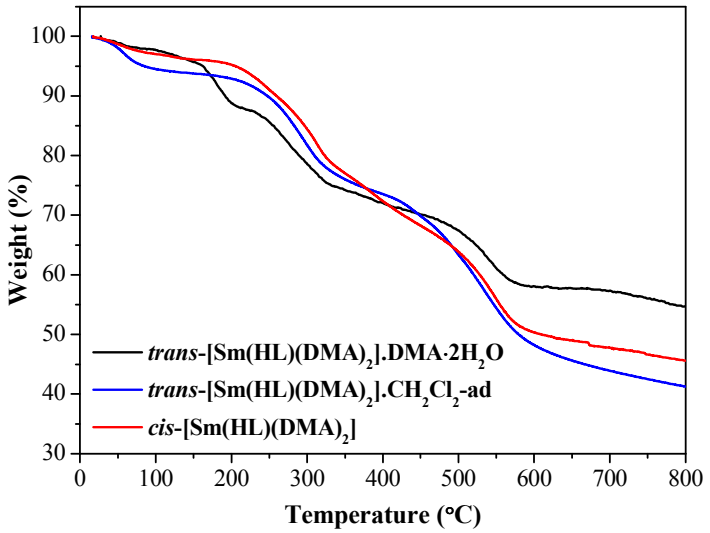

Figure S15. TGA profiles of *trans*-[Sm(HL)(DMA)$_2$]·DMA·2H$_2$O (black), *trans*-[Sm(HL)(DMA)$_2$]·CH$_2$Cl$_2$-ad (blue) and *cis*-[Sm(HL)(DMA)$_2$] (red). The PXRD shows that at the beginning of the TGA measurement, *trans*-[Sm(HL)(DMA)$_2$]·CH$_2$Cl$_2$-ad sample has a profile consistent with loss of volatile CH$_2$Cl$_2$ from an intermediate framework structure.

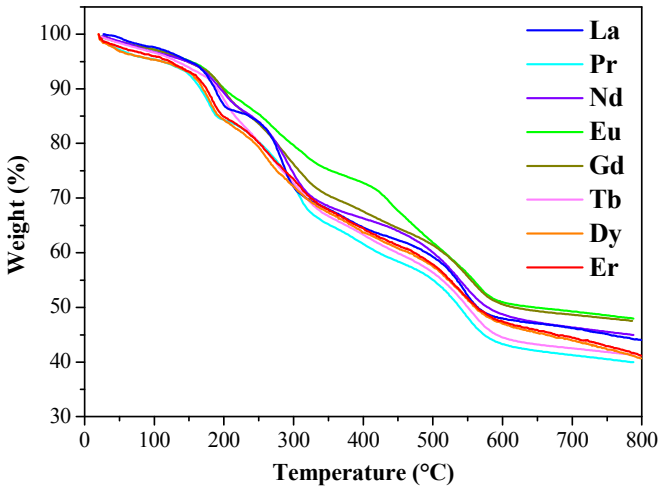

Figure S16. TGA profiles of 'as-synthesized' *trans*-[Ln(HL)(DMA)$_2$]·DMA·2H$_2$O (Ln = La, Pr, Nd, Eu, Gd, Tb, Dy, Er).

S5. Additional Gas Adsorption Isotherms

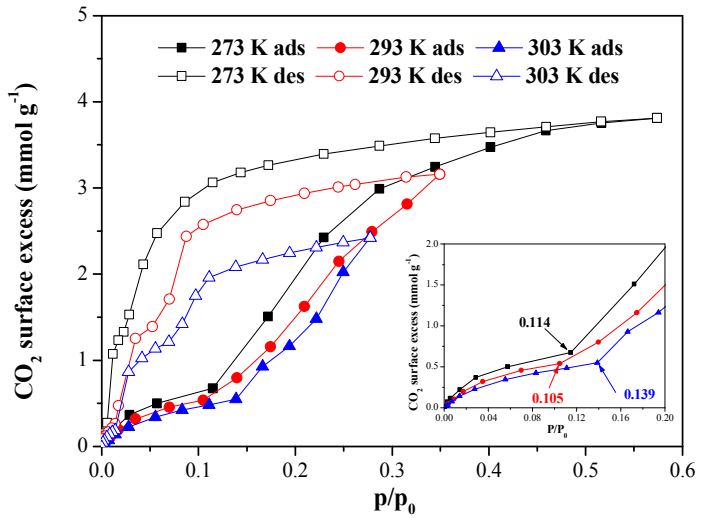

Figure S17. CO_2 adsorption/desorption isotherms as a function of relative pressure (Pressure range: 0 − 20 bar) for *cis*-[Sm(HL)(DMA)$_2$].

(a)

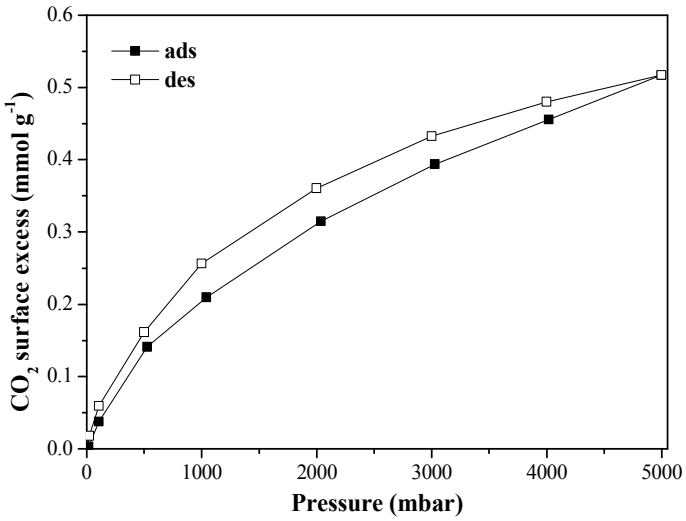

(b)

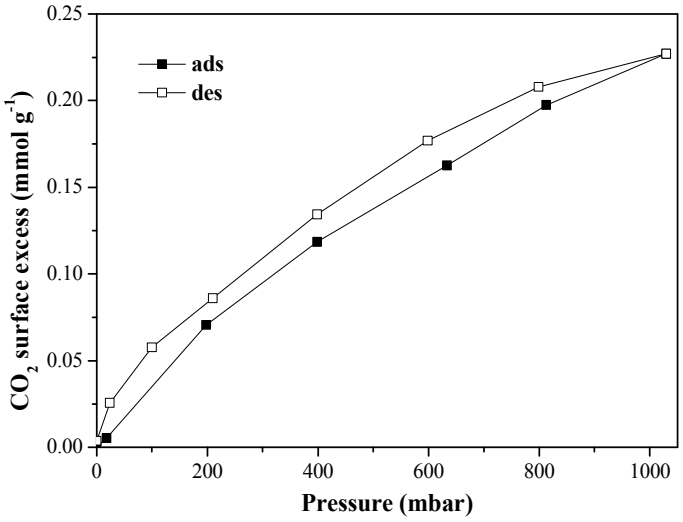

Figure S18. CO_2 adsorption/desorption isotherms for *cis*-[Sm(HL)(DMA)$_2$] at 293 K for pressures ranges (a) 0 − 5 bar and (b) 0 − 1 bar.

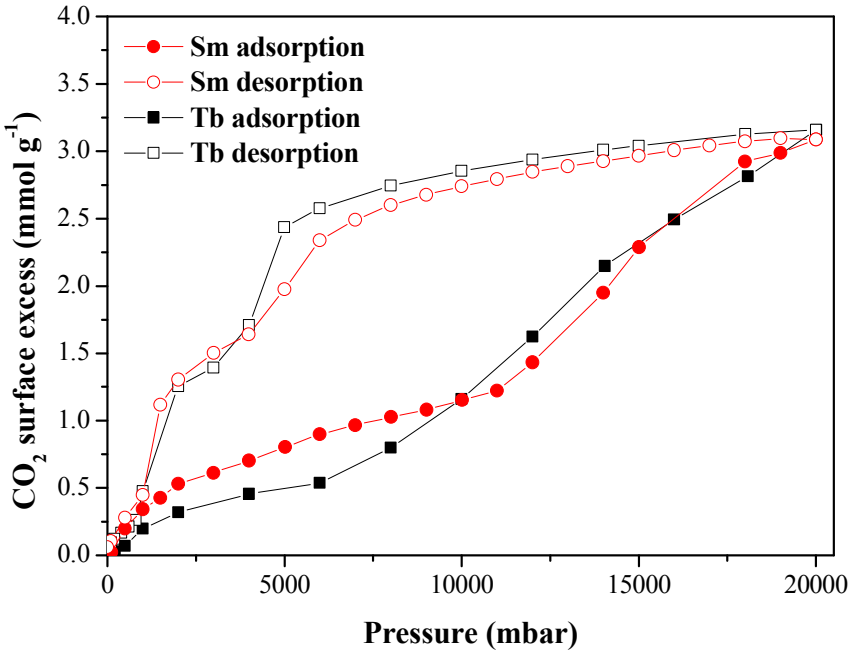

Figure S19. Comparison of CO_2 adsorption/desorption isotherms of *cis*-[Sm(HL)(DMA)$_2$] and *cis*-[Tb(HL)(DMA)$_2$] at 293 K.

S6. Thermodynamics Analysis for CO_2 Adsorption

The isosteric adsorption enthalpy of CO_2 was calculated using the Clausius-Clapeyron equation.

$$\frac{d(\ln(p))}{d(\frac{1}{T})} = \frac{Q_{st}}{R} \quad (1)$$

where p is pressure, T is the temperature, R is the real gas constant. At lower surface coverage (≤ 0.5 mmol g^{-1}), which is below the CO_2 uptake where the adsorption step starts, ln(p) and 1/T graphs were obtained from the CO_2 isotherms at 273, 293, 303, 313 and 333 K (Figure S20a). At higher surface coverage (≥ 0.7 mmol g^{-1}), which is above the CO_2 uptake capacity where the adsorption step starts, ln (p) and ln (1/T) graphs were obtained from the CO_2 isotherms at 273, 293, 303 and 313 K (Figure S20b). All the graphs have good linearity, indicating consistency of the isotherm data for the CO_2-host system over the temperature ranges studied. The calculated results of Q_{st} and ΔS were listed in Table S6 and plotted in Figure 7c.

(a)

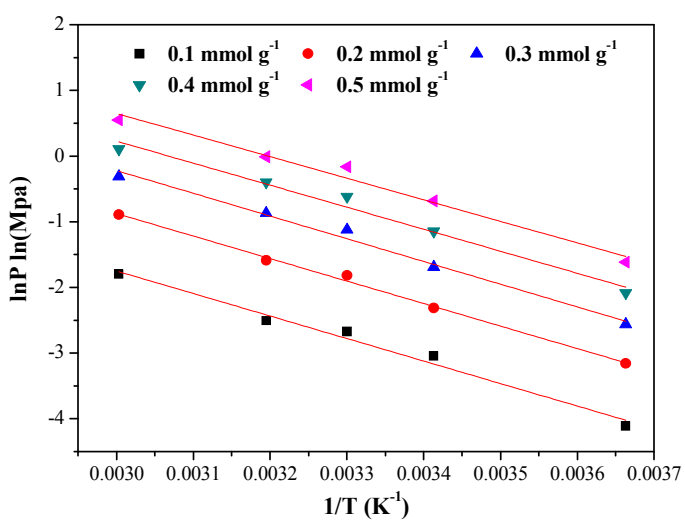

(b)

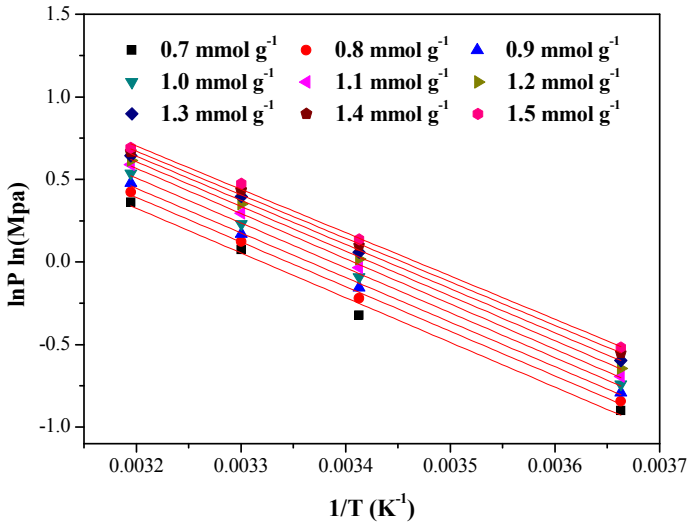

Figure S20. Graphs of ln(*p*) versus 1/T for the adsorption of CO_2 on *cis*-[Sm(HL)(DMA)$_2$] at 273−333 K (a) 0.1 − 0.5 mmol g^{-1} data for adsorption isotherms in the range 273 − 333 K and (b) 0.7−1.5 mmol g^{-1} data for adsorption isotherms in the range 273 − 313 K.

Table S6. The Isosteric Adsorption Enthalpies (Q_{st}) and Entropies (ΔS) of CO_2 for *cis*-[Sm(HL)(DMA)$_2$] as a function of various Amounts Adsorbed, Calculated for Isotherms over the Temperature Range 273 − 333 K.

CO_2 uptake (mmol g^{-1})	dln(p)/d(1/T)	Q_{st} (kJ mol^{-1})	Standard error (Q_{st})	ΔS (J K^{-1} mol^{-1})	Standard error (ΔS)
0.1	-3428.4	28.5	2.0	-71.0	6.7
0.2	-3428.0	28.5	1.0	-78.2	3.3
0.3	-3460.4	28.8	1.7	-84.5	5.7
0.4	-3353.2	27.9	2.1	-85.5	7.1
0.5	-3288.4	27.3	2.1	-87.4	7.0
0.7	-2709.2	22.5	1.4	-74.8	4.7
0.8	-2704.3	22.5	0.7	-75.2	2.5
0.9	-2702.0	22.5	0.6	-75.6	2.0
1.0	-2720.5	22.6	0.5	-76.6	1.6
1.1	-2739.8	22.8	0.4	-77.6	1.2
1.2	-2710.7	22.5	0.4	-77.2	1.2
1.3	-2675.7	22.3	0.5	-76.5	1.7
1.4	-2637.9	21.9	0.6	-75.8	2.1
1.5	-2622.7	21.8	0.7	-75.6	2.5

S7. Adsorption Kinetics Analysis for Temperature Swing Adsorption of CO_2

(a)

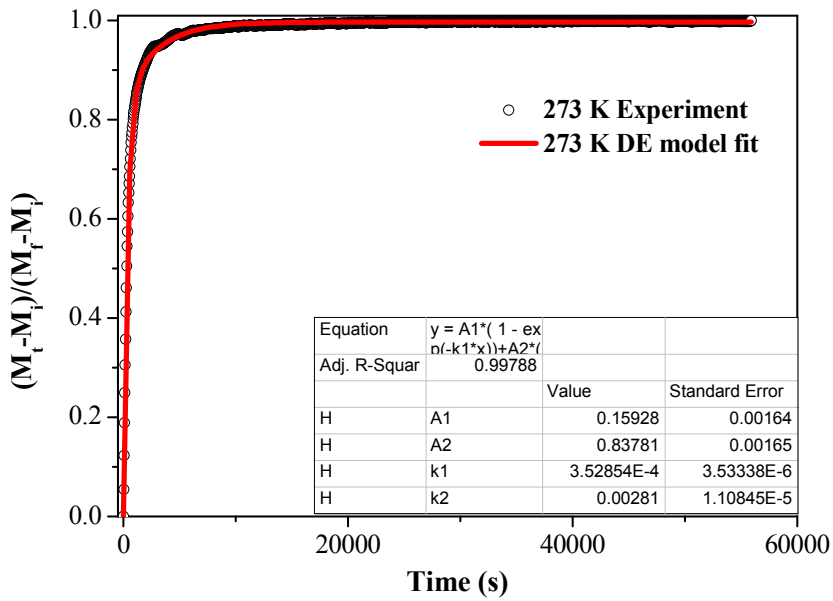

Equation	y = A1*(1 - exp(-k1*x))+A2*(		
Adj. R-Squar	0.99788		
		Value	Standard Error
H	A1	0.15928	0.00164
H	A2	0.83781	0.00165
H	k1	3.52854E-4	3.53338E-6
H	k2	0.00281	1.10845E-5

(b)

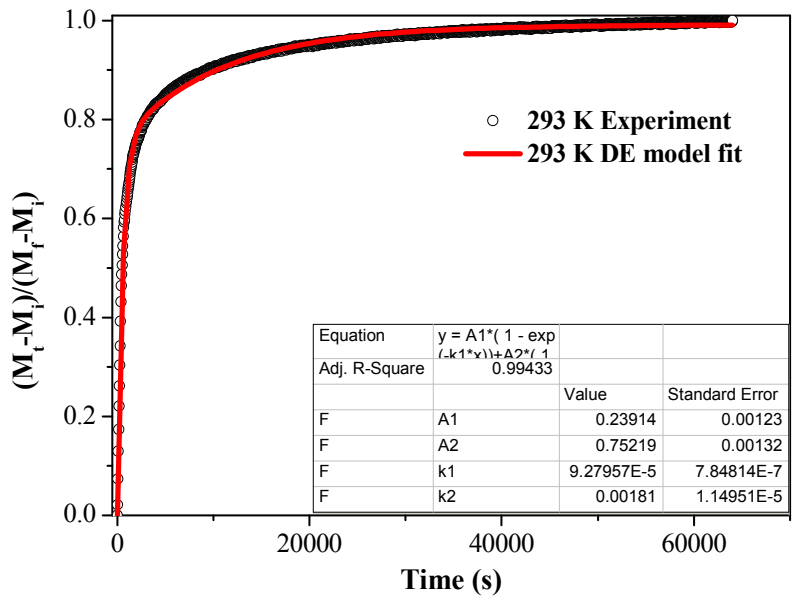

Equation	y = A1*(1 - exp(-k1*x))+A2*(1		
Adj. R-Square	0.99433		
		Value	Standard Error
F	A1	0.23914	0.00123
F	A2	0.75219	0.00132
F	k1	9.27957E-5	7.84814E-7
F	k2	0.00181	1.14951E-5

(c)

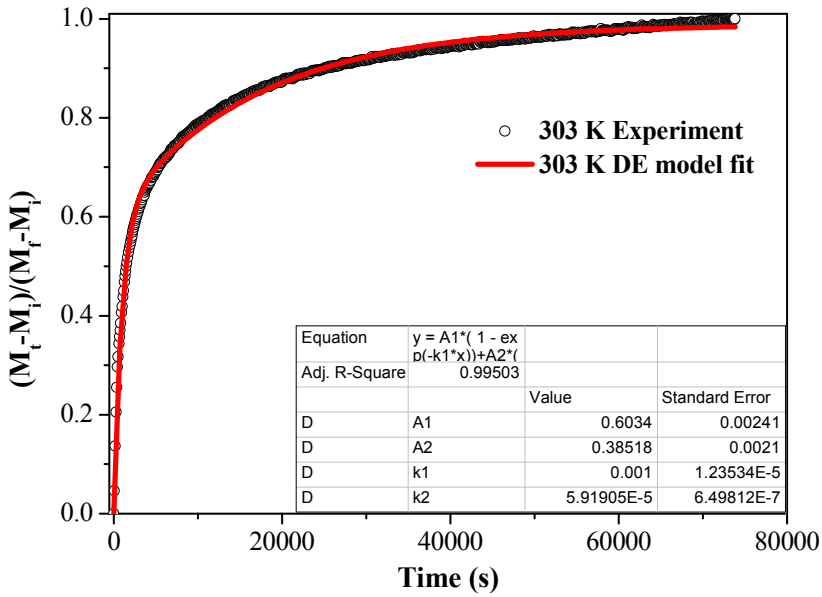
1.0
0.8
0.6
0.4
0.2
0.0
0
20000
40000
60000
80000
Time (s)
$(M_t-M_i)/(M_f-M_i)$
303 K Experiment
303 K DE model fit
Equation
y = A1*(1 - exp(-k1*x))+A2*(
Adj. R-Square
0.99503
Value
Standard Error
D A1 0.6034 0.00241
D A2 0.38518 0.0021
D k1 0.001 1.23534E-5
D k2 5.91905E-5 6.49812E-7

(d)

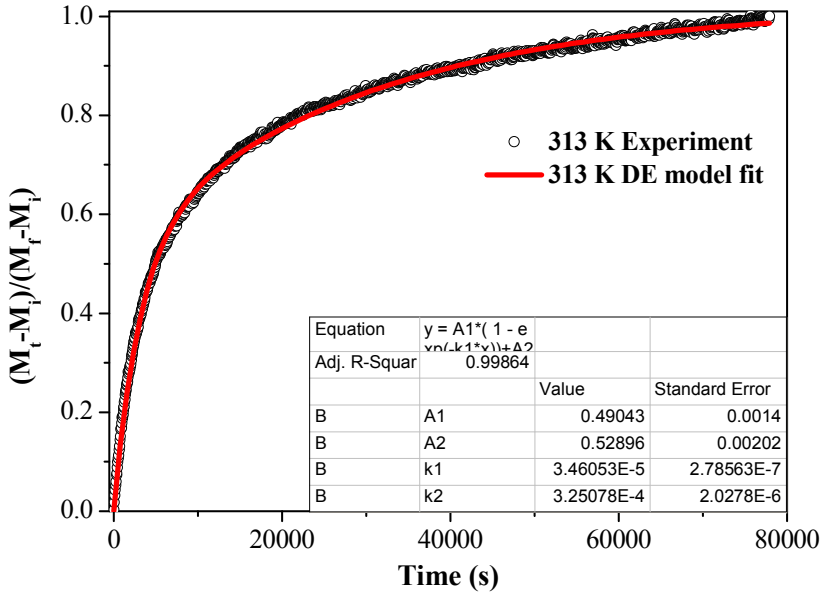
1.0
0.8
0.6
0.4
0.2
0.0
0
20000
40000
60000
80000
Time (s)
$(M_t-M_i)/(M_f-M_i)$
313 K Experiment
313 K DE model fit
Equation
y = A1*(1 - exp(-k1*x))+A2
Adj. R-Squar
0.99864
Value
Standard Error
B A1 0.49043 0.0014
B A2 0.52896 0.00202
B k1 3.46053E-5 2.78563E-7
B k2 3.25078E-4 2.0278E-6

(e)

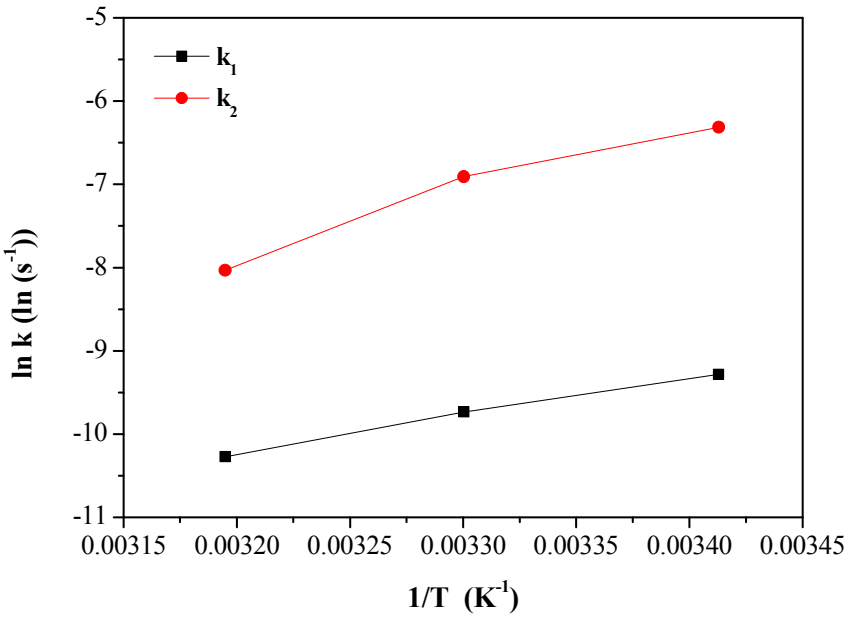

Figure S21. Double exponential (DE) model fitting graphs and kinetic parameters for *cis*-[Sm(HL)(DMA)$_2$] (a) 273 K, (b) 293 K, (c) 303 K, and (d) 313 K and (e) DE kinetic parameters versus 1/T

Table S7. Time of $(M_t\text{-}M_i)/(M_e\text{–}M_i) = 0.5$ ($t_{1/2}$) of *cis*-[Sm(HL)(DMA)$_2$] between 273 and 313 K

Temp. (K)	273	293	303	313
$t_{1/2}$ (s)	293	505	1515	4991

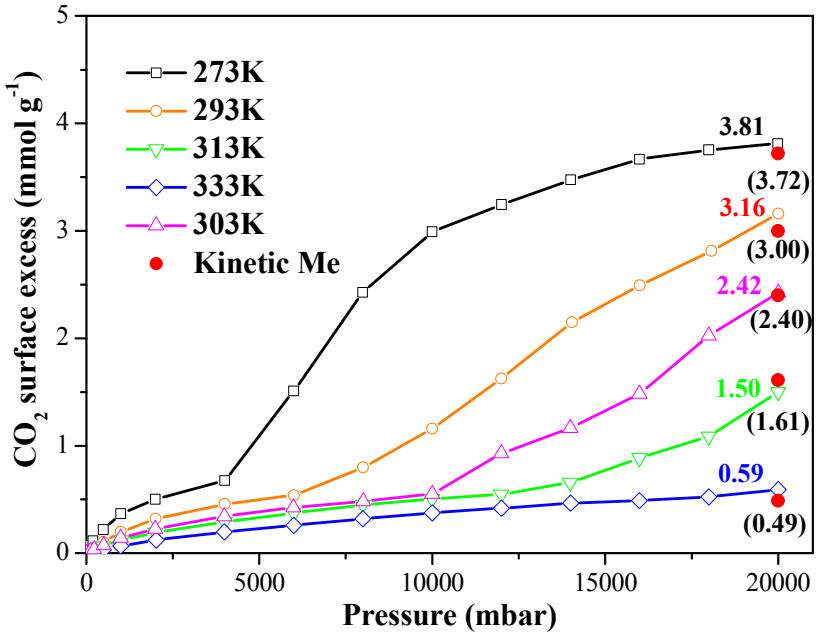

Figure S22. Comparison of final CO_2 uptake in kinetic profiles for *cis*-[Sm(HL)(DMA)$_2$] (● with black numbering in brackets) and isotherm surface excess uptakes(colored numbering).

Table S8. Comparison of Final CO_2 Uptake in Kinetic Profiles and Isotherm Surface Excess Uptakes for *cis*-[Sm(HL)(DMA)$_2$]

Temp. (K)	Isotherm (mmol g^{-1})	Kinetic Profile (mmol g^{-1})
273	3.81	3.72
293	3.16	3.00
303	2.42	2.40
313	1.50	1.61
333	0.59	0.49

Table S9. DE Model Fitting Results for *cis*-[Sm(HL)(DMA)$_2$] at 20 bar between 273 and 313 K

Temp. (K)	A_1	k_1 (10^{-4})	A_2	k_2 (10^{-3})
273	0.1593	3.53	0.8378	2.81
293	0.2391	0.928	0.7522	1.81
303	0.3852	0.592	0.6034	1.00
313	0.4904	0.346	0.5290	0.325

S8 Kinetic Profiles for Carbon Dioxide Adsorption on *cis*-[Sm(HL)(DMA)$_2$] at 273 K

(a)

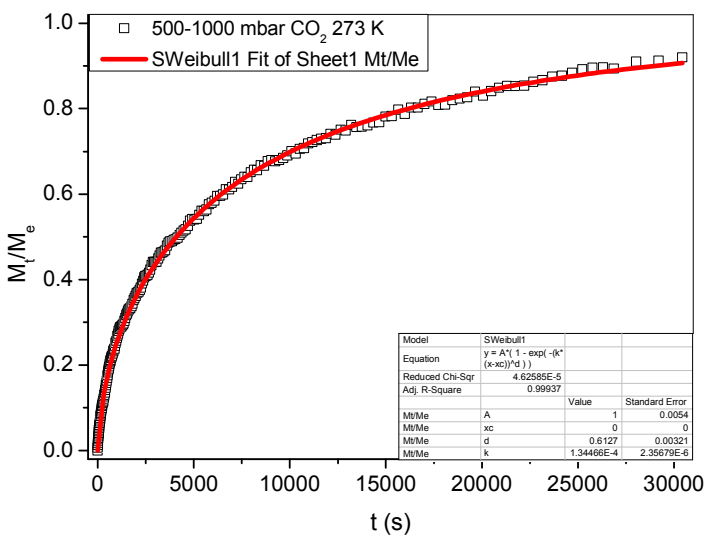

(b)

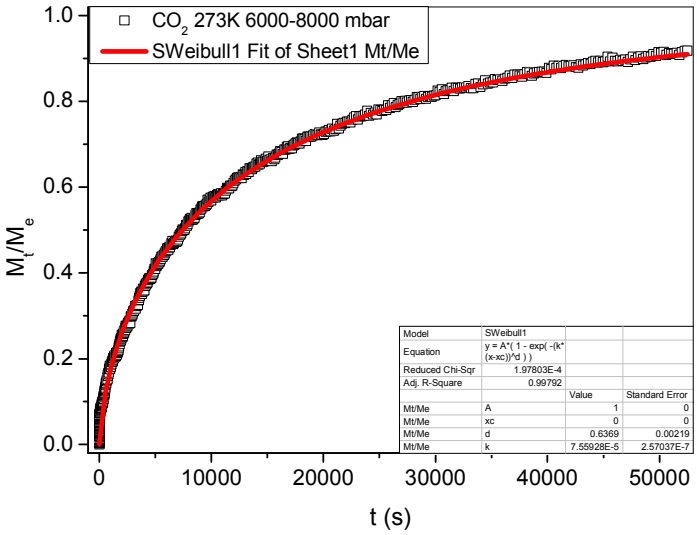

Figure S23 Kinetic profiles for various pressure Increments for carbon dioxide adsorption on *cis*-[Sm(HL)(DMA)$_2$] at 273 K, (a) 500−1000 mbar and (b) 6000−8000 mbar

S9 Comparison of Kinetic Profiles for Fickian diffusion into a Sphere, Cylinder and One-dimensional Slab with the Stretched Exponential Model

Theoretical Fickian profiles for diffusion into a cylinder and sphere were calculated using equations (3) and (4) in the main manuscript. Fickian diffusion into a one-dimensional slab is given by the equation below:[3]

$$\frac{M_t}{M_e} = 1 - \frac{8}{\pi^2}\sum_{n=0}^{\infty}\left(\frac{1}{(2n+1)^2}\right)\exp\left(\frac{-D(2n+1)^2\pi^2 t}{4w^2}\right) \qquad (2)$$

where M_t is mass uptake at time t , M_e is mass uptake at equilibrium, D is diffusivity and w is the half thickness of the parallel sided slab.[1]

(a) Sphere

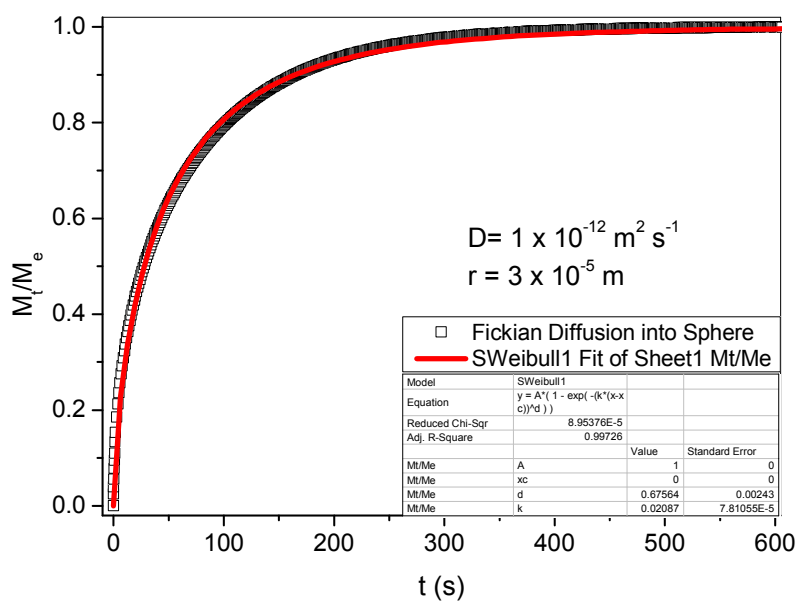

(b) Cylinder

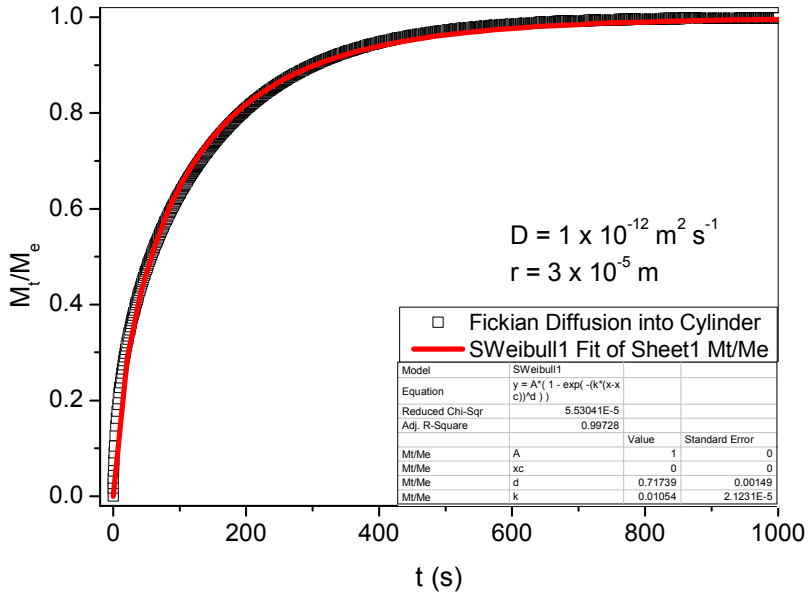

(c) 1-D Slab

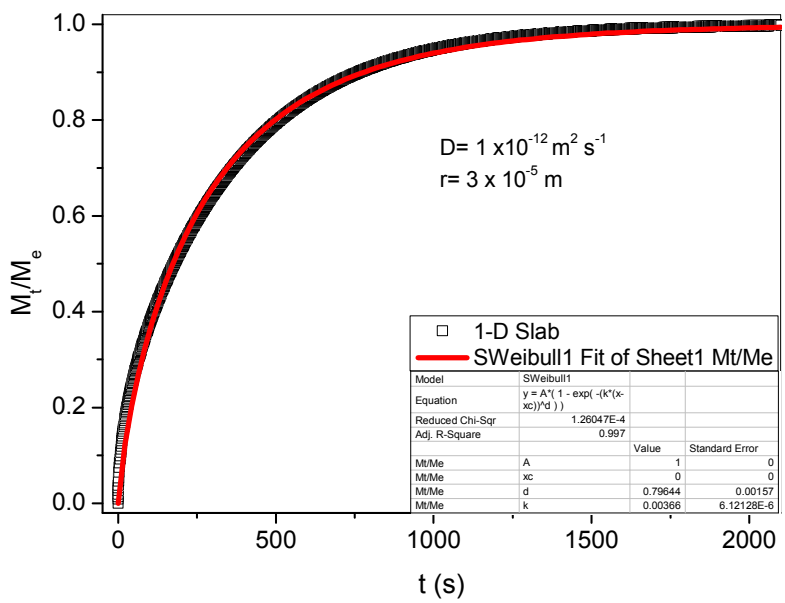

(d) Comparison

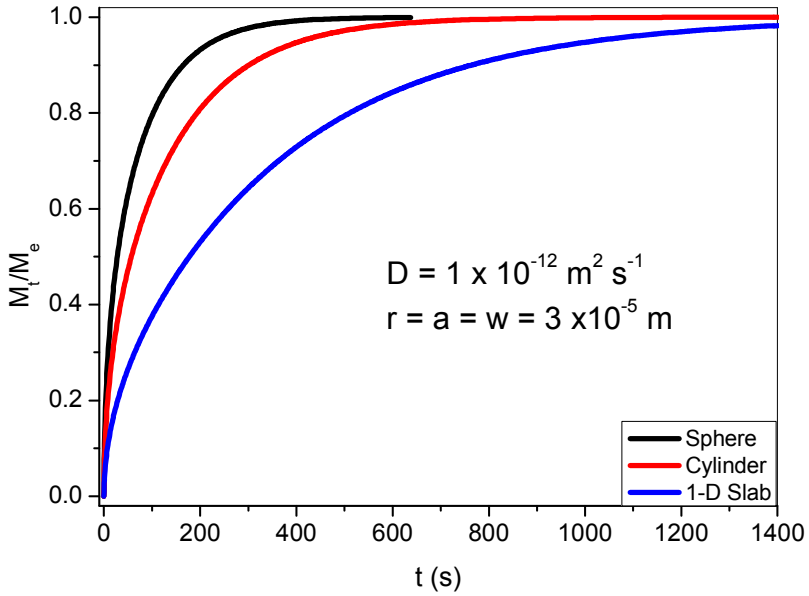

Figure 24. Comparison of theoretical Fickian profiles and corresponding fits to the Stretched Exponential Model (a) sphere,(b) cylinder and (c) one-dimensional slab and (d) comparison of diffusion curves for different shapes

Figures S23a-c show that for constant Diffusion Coefficient (1×10^{-12} m^2 s^{-1}) and r = a = w = 3×10^{-5} m, the shape of the kinetic profiles varies markedly with particle shape. Therefore, in the case of analysis of an experimental kinetic profile the diffusion coefficient will depend on the shape of the particle chosen in the analysis. However, the stretched exponential model provides excellent fits for Fickian diffusion into all shapes and the Linear Driving Force model is a special case of the Stretched Exponential Model. Furthermore, the stretched exponential model also fits kinetic profiles which do not fit Fickian diffusion (see Figure10a and Figure S23). The results clearly show that the stretched exponential model provides a good fit to theoretical curves for Fickian diffusion into particles with a wide variety of shapes and some non-Fickian cases.

S10. Calculation of Adsorption/Desorption Selectivity for Gas Adsorption

(a)

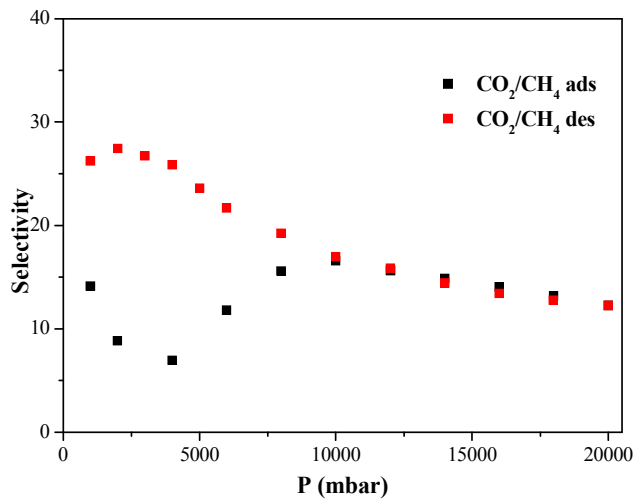

(b)

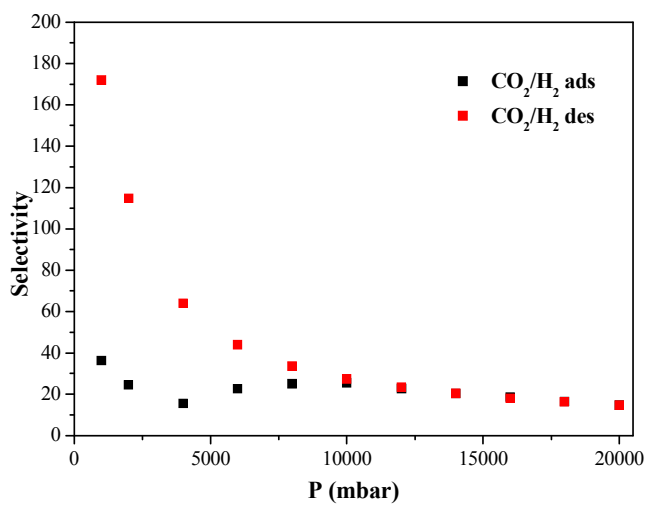

(c)

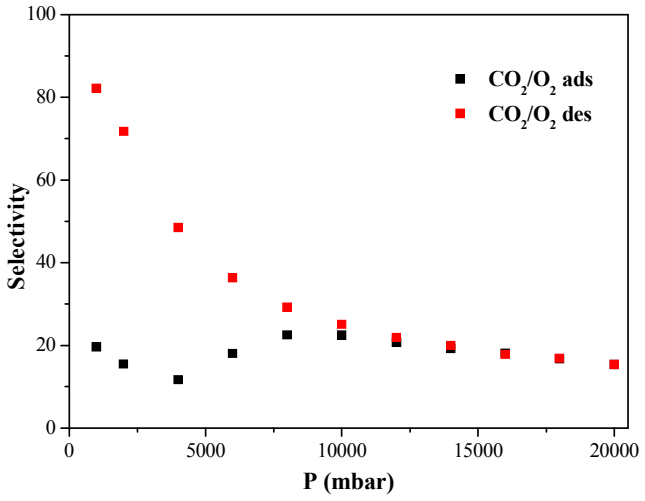

(d)

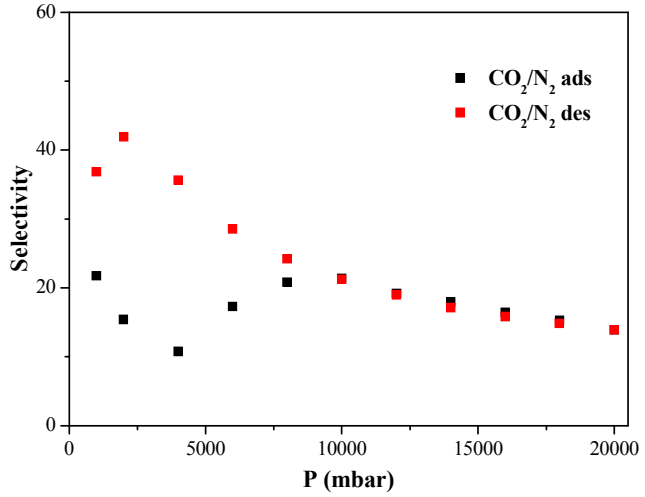

Figure S25 Single-component gas selectivity of *cis*-[Sm(HL)(DMA)$_2$] for (a) CO_2/CH_4, (b) CO_2/H_2, (c) CO_2/O_2, (d) CO_2/N_2, calculated from the isotherms at 273 K.

S11. Calculation of Henry's Law Selectivity for Gas Adsorption

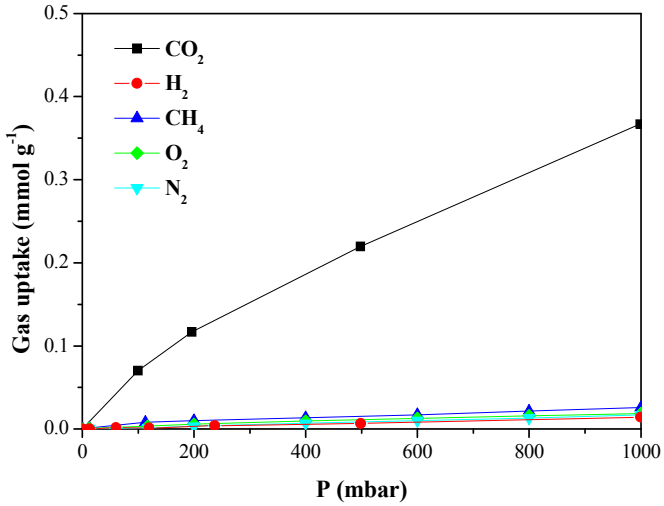

Figure S26. Comparison of CO_2, CH_4, H_2, O_2 and N_2 sorption isotherms for *cis*-[Sm(HL)(DMA)$_2$] up to 1.0 bar at 273 K.

(a)

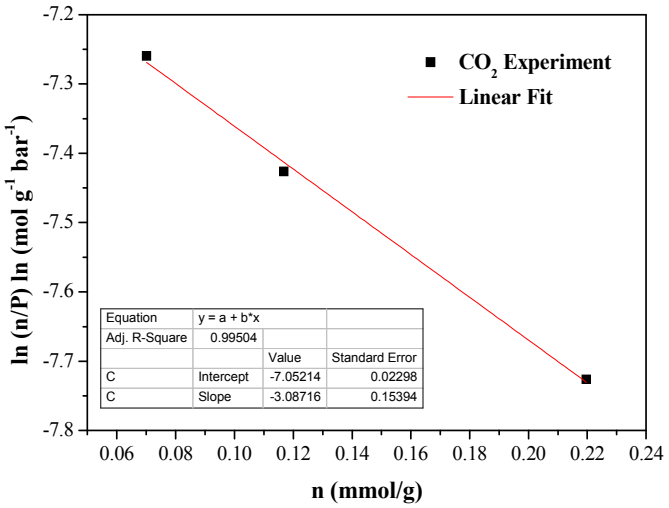

(b)

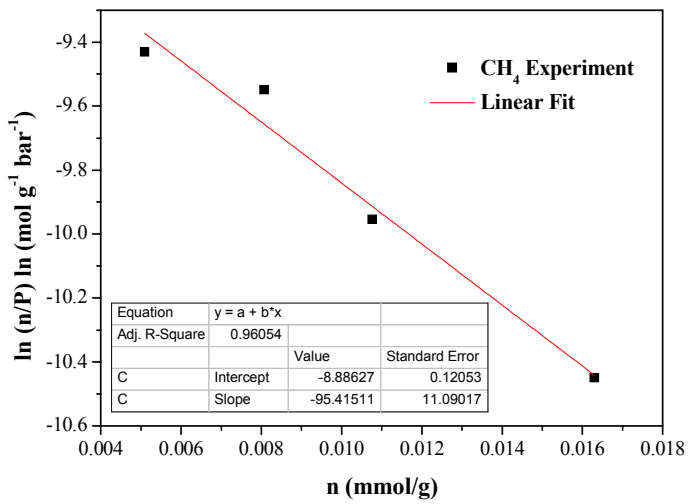
CH4 Experiment
Linear Fit
ln (n/P) ln (mol g-1 bar-1)
n (mmol/g)
-9.4
-9.6
-9.8
-10.0
-10.2
-10.4
-10.6
0.004
0.006
0.008
0.010
0.012
0.014
0.016
0.018
Equation | y = a + b*x
Adj. R-Square | 0.96054
Value | Standard Error
C | Intercept | -8.88627 | 0.12053
C | Slope | -95.41511 | 11.09017

(c)

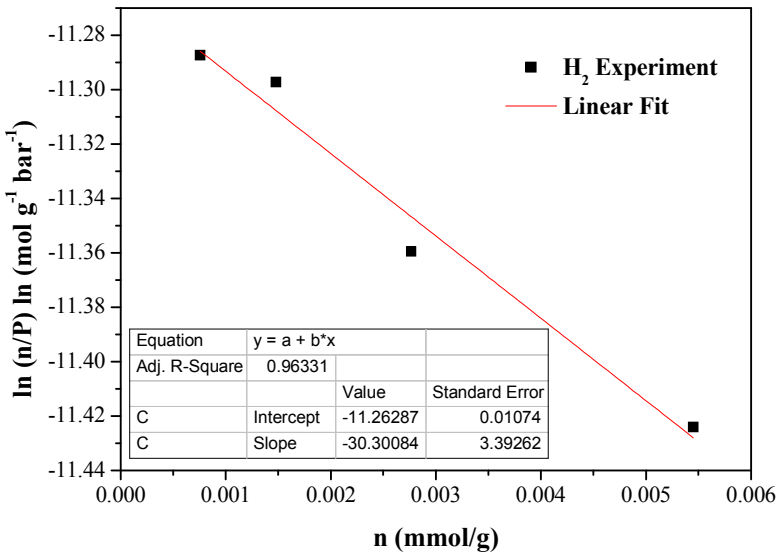
H2 Experiment
Linear Fit
ln (n/P) ln (mol g-1 bar-1)
n (mmol/g)
-11.28
-11.30
-11.32
-11.34
-11.36
-11.38
-11.40
-11.42
-11.44
0.000
0.001
0.002
0.003
0.004
0.005
0.006
Equation | y = a + b*x
Adj. R-Square | 0.96331
Value | Standard Error
C | Intercept | -11.26287 | 0.01074
C | Slope | -30.30084 | 3.39262

(d)

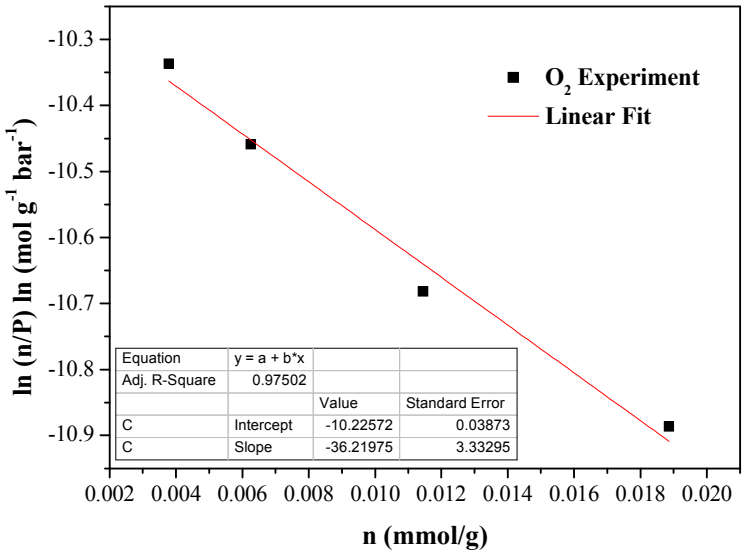

(e)

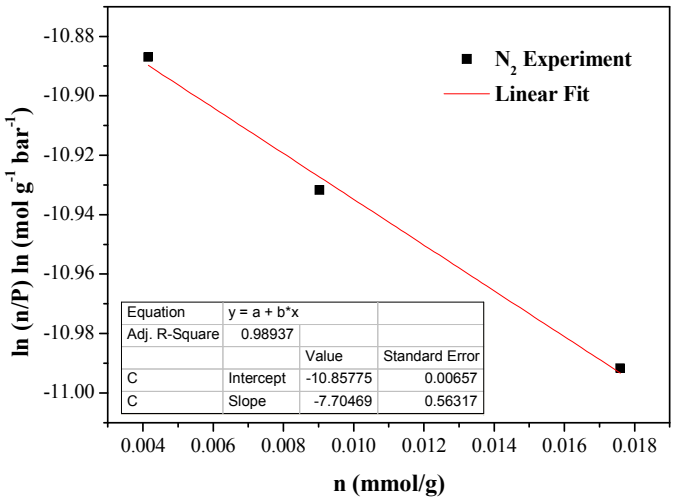

Figure S27. Linear Henry's Law graphs for (a) CO_2, (b) CH_4, (c) H_2, (d) O_2 and (e) N_2 adsorption isotherms for *cis*-[Sm(HL)(DMA)$_2$] at 273 K.

Table S10. Linear RegressionR and Henry's constants K_H for CO_2, CH_4, H_2, O_2 and N_2 Isotherm Data for *cis*-[Sm(HL)(DMA)$_2$] at 273 K.

	CO_2	CH_4	H_2	O_2	N_2
K_H/mol g^{-1} bar^{-1}	8.66×10^{-4}	1.38×10^{-4}	1.28×10^{-5}	3.62×10^{-5}	1.93×10^{-5}

Table S11. Comparison of the Selectivity Calculated from the Adsorption/desorption isotherms and Henry's Law Selectivity data from linear fitting results for *cis*-[Sm(HL)(DMA)$_2$] at 273 K.

Selectivity ratio	Adsorption Isotherm	Desorption Isotherm	Henry's Law analysis
CO_2/CH_4	17/1	27/1	6/1
CO_2/H_2	36/1	172/1	68/1
CO_2/O_2	22/1	82/1	24/1
CO_2/N_2	22/1	42/1	45/1

References

1) Sheldrick, G. M. SHELXL-97: Program for crystal structure refinement; University of Göttingen, Göttingen, Germany, 1997.
2) Lange's Handbook of Chemistry; 15th ed.; McGraw-Hill: New York, 1999.
3) Crank, J. *The Mathematics of Diffusion*; 2nd ed.; Clarendon Press: Oxford, 1975.